Factors controlling long-term phosphorus efflux from lake sediments: Exploratory reactive-transport modeling

Sergei Katsev *, Iana Tsandev [1], Ivan L'Heureux, Denis G. Rancourt

Lake Sediment Structure and Evolution Group, Department of Physics, University of Ottawa, 150 Louis Pasteur, Ottawa, Canada K1N 6N5

Abstract

We perform, for the first time, a global sensitivity analysis on a generic diagenetic reaction-transport model (RTM) to elucidate the effects of environmental, thermodynamic, and kinetic factors on the magnitudes of phosphorus release fluxes from aquatic sediments under a range of conditions typically found in lake sediments. Our model includes the processes that describe redox-sensitive phosphorus releases (the so-called classical model) and processes by which phosphorus mobilization is affected by porewater sulfate. On decadal and longer time scales, sediment phosphorus effluxes are primarily determined by: sedimentation flux of reactive organic matter, sedimentation flux of iron oxyhydroxides, concentrations of dissolved oxygen and sulfate at the sediment–water interface, and the rate at which phosphate is immobilized in reduced sediment. We show that the effects of these factors on phosphorus effluxes are interdependent and discuss the mechanisms of such interactions. The dominant pathways by which dissolved sulfate increases phosphorus efflux in iron-rich hypoxic sediments are discussed in detail. In contrast to short-term phosphorus releases, such as described by the classical model, long-term phosphorus retention is controlled by phosphorus removal to deep, reduced, sediment, rather than processes at the sediment–water interface. Hence, the results of short-term laboratory or in-situ studies (such as sediment incubations experiments) cannot be unequivocally extended to long time scales. Our results provide explanations to the reports that lake restoration measures such as restricting phosphorus inputs to a lake or oxygenating the lake's hypolimneon (or both) in the long-term often fail to decrease sediment phosphorus effluxes. The re-deposition of sediment substances after their release into the water column (the feedback often overlooked in sediment RTMs) can critically affect the magnitude and dynamics of phosphorus efflux from sediments. Depending on sediment history, the same set of external (boundary) conditions can generate diagenetic regimes with either high or low phosphorus effluxes (bistability).
© 2006 Elsevier B.V. All rights reserved.

Keywords: Phosphorus release; Lake sediments; Sensitivity analysis; Reactive-transport modeling; Lake restoration

1. Introduction

Retention of phosphorus in aquatic sediments is a major factor regulating the trophic state of the overlying waters in a wide variety of environments (Boström et al., 1982). Identifying how benthic phosphorus fluxes are determined by sediment characteristics and history is crucial for understanding and, ultimately, predicting and managing sediment phosphorus releases. Kinetic reactive-

---

* Corresponding author. Present address: Department of Earth and Planetary Sciences, McGill University, 3450 University Street, Montreal, Quebec, Canada H3A 2A7. Fax: +1 514 398 4680.

E-mail address: sergei@eps.mcgill.ca (S. Katsev).

[1] Present address: Department of Earth Sciences, Utrecht University, P.O. Box 80.021, 3508 TA Utrecht, The Netherlands.

transport models (RTMs) (Berner, 1980; Boudreau, 1997) are powerful and inexpensive, yet underutilized, tools for performing this task by exploring sediment early diagenesis under a variety of conditions. RTMs are continuous in space and time and describe complex interconnected webs of physical, chemical, and biogeochemical interactions in the sediment at the level of individual chemical reactions and transport processes. The model reactions and processes are characterized by kinetic parameters that are largely universal across different environments. By their construction, RTMs represent the current state of conceptual understanding of sediment diagenesis and thus make it possible to investigate sediment phosphorus controls by exploring model solutions corresponding to a variety of postulated model inputs — a practice that is especially beneficial where consistent measurements over an extended range of conditions are impossible or expensive.

Sensitivity analysis is the main tool for determining control factors and estimating result uncertainties in complex computational models with a large number of processes (Omlin et al., 2001). A local sensitivity analysis is most often performed whereby the effects of small variations in the model parameters are investigated for a selected state of the sediment system, typically the one for which the model is calibrated to the available data (Van Cappellen and Wang, 1996a). On the other hand, descriptions of benthic phosphorus fluxes over a range of sediment conditions, or over extended periods of time, require extrapolations beyond the model calibration range. The required "global" sensitivity analysis over an extended range of sediment conditions, is rarely performed (Tromp et al., 1995; Jourabchi et al., 2005) and no particular analysis method is currently recognized as standard (Brun et al., 2001; Omlin et al., 2001; Wang et al., 2003). No such analysis has been performed yet to identify control factors for sediment phosphorus releases.

In this paper, we perform both local and global sensitivity analyses on a diagenetic RTM to determine factors that most control long-term phosphorus effluxes from aquatic sediments. The global analysis is performed in a factorial design setup (Montgomery, 1997) that allows evaluating the importance of individual system characteristics, such as chemical species concentrations or reaction rate constants, as well as interrelations among their effects on phosphorus mobilization. In order to be specific, we restrict the analyses to long-term (steady-state) phosphorus effluxes under a range of conditions typically found in freshwater lake sediments.

We show that, in contrast to the classical model (Einsele, 1936; Mortimer, 1941) for short-term phospho-rus releases upon the onset of sediment anoxia, long-term phosphorus retention in sediments is relatively insensitive to the details of phosphorus cycling near the sediment–water interface and is determined mainly by the effectiveness of phosphorus retention in deep, reduced, sediment. We emphasize that the long-term phosphorus retention can be controlled by mechanisms that are different from the ones responsible for the short-term (e.g., seasonal) phosphorus releases. For this reason, the results of short-term laboratory or in-situ studies (such as sediment incubations experiments) cannot be unequivocally extended to characterize phosphorus retention mechanisms on longer time scales or to devise long-term phosphorus retention strategies. We show that feedback interactions between the sediment and the water column can critically affect the magnitude and dynamics of the phosphorus efflux from sediments and illustrate how restricting phosphorus inputs to a lake or oxygenating the lake's hypolimnion may be ineffective in decreasing phosphorus effluxes from sediment after a prolonged period of eutrophication. We also describe the mechanisms by which dissolved sulfate may significantly affect benthic phosphorus fluxes in iron-rich sediments, even at the relatively low concentrations found in lakes.

The paper is organized as follows. First, we briefly review the proposed mechanisms for sediment phosphorus mobilization and describe the processes that are included in our model, which is subsequently presented. Then we describe the factorial sensitivity analysis method, illustrate representative model solutions and present the analysis results. We next discuss the identified dominant phosphorus release mechanisms and analyze the differences between phosphorus release mechanisms on short and long time scales. The effects of coupling between the sediment and the water column are discussed. The last section summarizes our findings.

2. Phosphorus release mechanisms

The magnitude and timing of phosphorus releases from aquatic sediments (Boström et al., 1982; Søndergaard et al., 2001) are affected by a multitude of factors, none of which is universally dominant (Holdren and Armstrong, 1980; Caraco et al., 1991; Boers et al., 1998). The so-called classical model (Einsele, 1936; Mortimer, 1941) is most commonly invoked to describe seasonal phosphorus releases at the onset of anoxia in the water overlying the sediment. The classical model links sediment phosphorus efflux to redox conditions at the sediment–water interface that are effectively controlled by the dissolved oxygen concentration in bottom water. When the sediment

surface is oxic, strong adsorption of dissolved phosphate to solid iron oxyhydroxides limits phosphorus efflux by preventing phosphate diffusion into the water column from deeper, reduced, sediment. Under anoxic conditions, iron oxyhydroxides reductively dissolve and phosphate is released into the water column.

The apparent success of the classical model resulted in a widespread attribution of phosphorus mobilization incidents to sediment redox conditions for a variety of situations and time scales (Prairie et al., 2001; Gächter and Müller, 2003). However, failures of the classical model were documented in a number of cases (Caraco et al., 1991). For example, a decade-long artificial oxygenation of a lake's hypolimneon was ineffective in increasing phosphorus retention in a sediment of a Swiss lake (Gächter and Wehrli, 1998; Gächter and Müller, 2003). A number of alternative phosphorus release controls were suggested, including redox-sensitive uptake and release of phosphorus by benthic bacteria (Gächter et al., 1988), phosphorus binding with calcium carbonates (House et al., 1986; Boers et al., 1998), and apatite precipitation (Golterman, 2001). Other factors potentially influencing sediment phosphorus retention include: the pH of the overlying water (by affecting the strength of ionic phosphate sorption to sediment solid surfaces), quantity and quality of the organic carbon input, inputs of phosphorus-bearing minerals, bioturbation, epipelic photosynthesis, rooted plant activity, in-sediment concentrations of organic matter, reactive iron, dissolved sulfate, and calcite, and other sediment characteristics (Wetzel, 2001).

Among the alternative phosphorus release mechanisms, a sulfate-controlled phosphorus mobilization (Mortimer, 1941; Caraco et al., 1993; Gächter and Müller, 2003) was suggested to explain several apparent deviations from classical model behaviors. Sulfur diagenesis is often neglected in freshwater environments because of the low sulfate concentrations. However, sulfate reduction rates in eutrophic lakes can approach those in brackish environments because of the rapid turnover between reduced and oxidized sulfur species (Holmer and Storkholm, 2001). It was suggested (Caraco et al., 1989; Roden and Edmonds, 1997) that dissolved sulfate can affect phosphorus efflux from sediments primarily by two mechanisms: 1) mobilization of the iron-bound phosphate when ferric oxyhydroxides are reductively dissolved by H_2S generated by sulfate reduction, and 2) prevention of phosphorus immobilization into ferrous minerals, such as vivianite, as a result of porewater iron depletion by iron monosulfide (FeS) precipitation. In addition, phosphorus can be mobilized as a result of a direct dissolution of

vivianite by H_2S (Roden and Edmonds, 1997; Gächter and Müller, 2003). The magnitude of the sulfate effect on phosphorus mobilization and the relative roles of the above mechanisms are still unclear in natural sediments, as none of these mechanisms have been directly demonstrated or quantified in situ.

3. The model

3.1. Reactions and transport processes

Our RTM (numerical code LSSE-Mega can be obtained at http://www.eps.mcgill.ca/~sergei/lssemega/ or by request to the corresponding author; Katsev et al., 2006) solves a set of diagenetic equations for the concentrations $C_i(x,t)$ of solid (in mol per gram of dry weight (DW)) and dissolved (in mol/cm^3) chemical species in the sediment:

$$\frac{\partial \xi C_i}{\partial t} = \frac{\partial}{\partial x}\left(\xi D_i \frac{\partial C_i}{\partial x}\right) - \frac{\partial}{\partial x}(\xi U_i C_i) + \sum_j \xi R_j. \qquad (1)$$

Here, t is time and x is the depth coordinate from the sediment–water interface down. U_i is the advection (burial) velocity. The factor ξ is equal to the sediment porosity φ for dissolved species and $(1-\varphi)\rho$ for solid species, where ρ is the grain density of dry sediment in g/cm^3. The effective diffusion coefficients D_i were calculated as sums of the bioturbation coefficient D_b and the appropriate molecular diffusion coefficients (corrected for sediment porosity using Archie's law and for temperature T using expressions in Boudreau (1997) for $T=5$ °C). The rate constants for the rates R_j of chemical and biochemical reactions (Tables 1–3) were taken from dSED, a database for modeling sediment diagenesis (Katsev et al., 2004). The reaction set in Table 1 was selected to reflect phosphorus release mechanisms in the classical model (reactions 1, 2, 5, 6, and 17) and sulfate-assisted phosphorus mobilization (reactions 3, 7–12, 14, 15).

Microbial decomposition of organic matter (OM) (represented by a nominal composition $(CH_2O)(NH_3)_y$ $(H_3PO_4)_z$ in reactions 1–4, Table 1) via a standard cascade of electron acceptors (Froelich et al., 1979) is described by Monod kinetics (Boudreau, 1996) (Table 2). Inhibition constants C_i^{inh} were assumed equal to the Monod constants C_i^{lim} for the respective species, for simplicity. The kinetics of the redox reactions between the products of reactions 1–4 are assumed second order (Table 2). Mineral precipitation and dissolution rates are taken to be proportional to the respective super- or

Table 1
Model reactions 'S–X' denotes a species X sorbed to a site S- on solid substrate surface; R' are dissolution rates

No.	Kinetic reactions	Rates
	Primary redox reactions	
1.	$(CH_2O)(NH_3)_y(H_3PO_4)_z + (1+2y)O_2 \rightarrow CO_2 + yNO_3^- + yH^+ + zH_3PO_4 + (1+y)H_2O$	R_{O2}
2.	$(CH_2O)(NH_3)_y(H_3PO_4)_z + 4Fe(OH)_3 + 7CO_2 \rightarrow 4Fe^{2+} + 8HCO_3^- + yNH_3 + zH_3PO_4 + 3H_2O$	$R_{Fe(OH)3}$
3.	$(CH_2O)(NH_3)_y(H_3PO_4)_z + 1/2SO_4^{2-} \rightarrow HCO_3^- + 1/2H_2S + yNH_3 + zH_3PO_4$	R_{SO4}
4.	$(CH_2O)(NH_3)_y(H_3PO_4)_z \rightarrow 1/2CH_4 + 1/2CO_2 + yNH_3 + zH_3PO_4$	R_{CH4}
	Secondary redox reactions	
5.	$4Fe^{2+} + O_2 + 8HCO_3^- + 2H_2O \rightarrow 4Fe(OH)_3 + 8CO_2$	R_{FeOx}
6.	$4S-Fe^+ + O_2 + 4HCO_3^- + 6H_2O \rightarrow 4S-H^0 + 4Fe(OH)_3 + 4CO_2$	R_{surFe}
7.	$H_2S + 2O_2 + 2HCO_3^- \rightarrow SO_4^{2-} + 2CO_2 + 2H_2O$	R_{SOx}
8.	$FeS + 2O_2 \rightarrow Fe^{2+} + SO_4^{2-}$	R_{FeSOx}
9.	$2Fe(OH)_3 + H_2S + 4CO_2 \rightarrow 2Fe^{2+} + S^0 + 4HCO_3^- + 2H_2O$	R_{SFe3}
10.	$Fe_3(PO_4)_2 + 3H_2S \rightarrow 3FeS + 2H_3PO_4$	R_{Sviv}
11.	$FeCO_3 + H_2S \rightarrow FeS + CO_2 + H_2O$	R_{SFeCO3}
12.	$FeS + H_2S \rightarrow FeS_2 + H_2$	R_{FeSHS}
13.	$2Fe(OH)_3 + FeS + 6CO_2 \rightarrow 3Fe^{2+} + S^0 + 6HCO_3^-$	R_{FeSFe3}
	Mineral precipitation reactions	
14.	$Fe^{2+} + HCO_3^- + HS^- \leftrightarrow FeS + CO_2 + H_2O$	R_{FeS}/R'_{FeS}
15.	$3Fe^{2+} + 2H_3PO_4 + 8H_2O \leftrightarrow Fe_3(PO_4)_2 \!*\! 8H_2O + 6H^+$	R_{viv}/R'_{viv}
16.	$xFe^{2+} + (1-x)Ca^{2+} + 2HCO_3^- \leftrightarrow Fe_xCa_{(1-x)}CO_3 + CO_2 + H_2O (x=1)$	R_{FeCO3}/R'_{FeCO3}
	Local equilibrium reactions	
	Adsorption	
17.	$H_3PO_4 \leftrightarrow H_3PO_4$ (ads)	
18.	$S-H^0 + Fe^{2+} + HCO_3^- \leftrightarrow S-Fe^+ + CO_2 + H_2O$	

Acid-base reactions	*Equilibrium constants*
$CO_2(aq) + H_2O \leftrightarrow HCO_3^- + H^+$	$K_{C1} = [H^+][HCO_3^-]/[CO_2]$
$HCO_3^- \leftrightarrow CO_3^{2-} + H^+$	$K_{C2} = [H^+][CO_3^{2-}]/[HCO_3^-]$
$H_2S \leftrightarrow HS^- + H^+$	$K_{HS} = [H^+][HS^-]/[H_2S]$
$H_2O \leftrightarrow H^+ + OH^-$	$K_W = [H^+][OH^-]$

under-saturations Ω_i (Table 2). Given the form of the OM decomposition rate expressions (Table 2), the overall rate of dissolved phosphate production from OM is determined by the OM concentration [OM] (i.e., OM-limited) and is equal to $zk_{OM}[OM]$, where k_{OM} is the rate constant, and z is the P:C ratio (c.f. Van Cappellen and Wang, 1996b). For the special case of depth-independent bioturbation, constant porosity φ and advection velocity U, the rate of phosphate primary production then decreases exponentially with depth as

$zk_{OM}[OM]^0 \exp(-ax)$, where $a = [(4\,D_b k_{OM} + U^2)^{1/2} - U]/(2D_b)$.

Reactive iron oxyhydroxide phases such as ferrihydrite (nominally $Fe(OH)_3$) and goethite (α-FeOOH) are represented by a single effective phase with stoichiometry $Fe(OH)_3$ (Tables 1 and 2). Similarly, the iron-phosphate mineral vivianite ($Fe_3(PO_4)_2$) effectively represents all sediment ferrous iron-phosphate minerals and amorphous solid phases. The parameter $\alpha = 1/5$ in the vivianite precipitation rate expression R_{viv} (Table 2)

Table 2
Kinetic reaction rate expressions used in the model

k_i are rate constants and k_{FeS}, K_{viv}, K_{FeCO3} are solubility constants

Primary redox reactions

For $i = \{O_2, Fe(OH)_3, SO_4, CH_4\}$,

$R_i = k_{OM}[OM]f_i$,

where $f_i = \dfrac{C_i}{C_i + C_i^{lim}} \displaystyle\prod_{j=1}^{i-1} \dfrac{C_j^{inh}}{C_j + C_j^{inh}}$, for i,j

$\qquad = \{O_2, Fe(OH)_3, SO_4\}$,

$\quad f_{CH_4} = 1 - \displaystyle\sum_j f_j$

Secondary redox reactions

$R_{FeOx} = k_{FeOx}[Fe^{2+}][O_2]$
$R_{SOx} = k_{SOx}[TS][O_2]$
$R_{SFe3} = k_{SFe3}[TS][Fe(OH)_3]$
$R_{Sviv} = k_{Sviv}[TS][\,Fe_3(PO_4)_2]$
$R_{SFeCO3} = k_{SFeCO3}[TS][FeCO_3]$
$R_{FeSOx} = k_{FeSOx}[FeS][O_2]$
$R_{surFe} = k_{surFe}[ads\text{-}Fe][O_2]$
$R_{FeSHS} = k_{FeSHS}[FeS][TS]$
$R_{FeSFe3} = k_{FeSFe3}[Fe(OH)_3][FeS]$

Mineral precipitation reactions

$R_{FeS} = k_{FeS}(\Omega_{FeS} - 1)\delta(\Omega_{FeS} - 1)$
$R'_{FeS} = k'_{FeS}[FeS](1 - \Omega_{FeS})\delta(1 - \Omega_{FeS})$

where $\Omega_{FeS} = \dfrac{[Fe^{2+}_{diss}][HS^-]}{K_{FeS}[H^+]}$ and $[HS^-] = \dfrac{[TS]}{1 + [H^+]/K_{HS}}$

$R_{viv} = k_{viv}(\Omega_{viv}^\alpha - 1)\delta(\Omega_{viv} - 1)$
$R'_{viv} = k'_{viv}[Fe_3(PO_4)_2](1 - \Omega_{viv}^\alpha)\delta(1 - \Omega_{viv})$,

where $\Omega_{viv} = \dfrac{[Fe^{2+}]^3[P_{diss}]^2}{K_{viv}}$ and $\alpha \approx 1/5$

$R_{FeCO3} = k_{FeCO3}(\Omega_{FeCO3} - 1)\delta(\Omega_{FeCO3} - 1)$
$R'_{FeCO3} = k'_{FeCO3}[FeCO_3](1 - \Omega_{FeCO3})\delta(1 - \Omega_{FeCO3})$

where $\Omega_{FeCO3} = \dfrac{[Fe^{2+}][CO_3^{2-}]}{K_{FeCO3}}$ and $[CO_3^{2-}]$

$\qquad = \dfrac{[TC]}{1 + [H^+]/K_{C2} + [H^+]^2/K_{C1}K_{C2}}$

Here, $\delta(x) = 1$ for $x > 0$ and $\delta(x) = 0$ for $x \le 0$.

was chosen from dimensional considerations (Lasaga, 1998), for the lack of better information.

The depth dependence of the bioturbation coefficient, $D_b(x)$, is approximated by

$$D_b = D_b^0 \frac{1 - \tanh(x - H)/\tau}{1 - \tanh(-H/\tau)}, \qquad (2)$$

where D_b^0 is the value at the sediment surface, $H = 5$ cm is the depth of the steepest gradient of $D_b(x)$ within the sediment and $\tau = 2$ cm is the characteristic depth half-interval within which most of the decrease in D_b occurs (Katsev et al., 2006). For simplicity, we neglected the D_b dependence on the sediment temperature and oxygen concentration, as well as the differences between the

bioturbation rates for solid and liquid species (Fossing et al., 2004). Also, the sediment porosity φ was assumed constant in space and time (no compaction), in which case the advection velocity U is the same for solid and liquid species and equals the sedimentation rate (in cm/yr) (Berner, 1980).

3.2. Adsorption

Reversible sorption of the ferrous iron ion on sediment solid surfaces is described by a pH-dependent equilibrium partitioning coefficient K_{adsFe} approximated by a Langmuir isotherm:

$$[ads - Fe] = K_{adsFe}[Fe^{2+}], \qquad (3)$$

where

$$K_{adsFe} = \sum_i \frac{K_{Fe,i}^* X_i S_{Ti}(1 - \gamma_i)}{[H^+] + K_{Fe,i}^*[Fe^{2+}]}. \qquad (4)$$

Here, square brackets denote the concentrations of the respective species and the sum runs over two types of solid substrates: ferric oxyhydroxides ($Fe(OH)_3$), and a "background" (B) which collectively represents all other sediment solids. Ferric oxyhydroxides are singled out because of their high specific sorption capacity for phosphate (Parfitt, 1989) and their susceptibility to redox-driven dissolution/precipitation that are central to the classical model of phosphorus release (Boström et al., 1988). [ads-Fe] is the concentration of adsorbed Fe (in mol/g_{DW}), X_i is the weight fraction of the i-th adsorption substrate ($i = 1,2$), S_{Ti} is the density (in mol/g_{DW}) of sorption sites at the substrate surface, and γ_i is the fraction of those sites that are occupied by other ions (c.f. Balistrieri and Murray, 1981; Van Cappellen and Wang, 1996b). The constants $K_{Fe,i}^*$ (Table 3) character-ize specific sorption capacities of the substrates. The term [H⁺] accounts for the pH-driven increase in K_{adsFe} within a pH interval roughly extending from 5 to 7.

By analogy, the adsorption coefficient for phosphate K_{adsP} is defined as

$$[ads - P] = K_{adsP}[P_{diss}] \qquad (5)$$

where

$$K_{adsP} = \sum_i \frac{K_{P,i}^* X_i S_{Ti}(1 - \gamma_i)}{[OH^-] + K_{P,i}^*[P_{diss}]}. \qquad (6)$$

Here, $[P_{diss}]$ is the aqueous total (all ionic species combined) phosphate concentration (in mol/cm³) and [ads-P] is the concentration of adsorbed phosphate (in mol/g_{DW}). A more rigorous derivation that takes into

Table 3
Parameter values used in the model

Parameter	Value	Units	Typical values	Refs.*
L	10	cm		
ρ	2.5	g cm^{-3}		
φ	0.8	–	0.7–0.95	a,b
U	0.2	cm yr^{-1}		
z (P:C)	0.005	–	0.002–0.016	c
$[O_2]^0$	1×10^{-7}	mol cm^{-3}	$(0–5) \times 10^{-7}$	d
$[SO_4]^0$	2×10^{-7}	mol cm^{-3}	$(1–200) \times 10^{-7\dagger}$	a,e
$[TC]^0$	2.44×10^{-6}	mol cm^{-3}		
$[ALK]^0$	2.3×10^{-6}	mol cm^{-3}		
F_{OM} ($=\Phi_{sed}/z$)	2.57×10^{-3}	mol cm^2 yr^{-1}		
F_{OM} ($=\Phi_{ext}/z$)	0.8×10^{-3}	mol cm^2 yr^{-1}		
$F_{Fe(OH)3}$	3.75×10^{-5}	mol cm^{-2} yr^{-1}		
k_{OM}	0.9	yr^{-1}		
C_{O2}^{lim}	2.0×10^{-10}	mol cm^{-3}	$10^{-10}–10^{-8}$	f,g
C_{SO4}^{lim}	4.0×10^{-7}	mol cm^{-3}	$10^{-9}–10^{-6}$	f
$C_{Fe(OH)3}^{lim}$	2.0×10^{-5}	mol g^{-1}	$10^{-10}–10^{-4}$	f,g
k_{FeOx}	0.35×10^{11}	cm^3 mol^{-1} yr^{-1}		f
k_{SOx}	1.6×10^8	cm^3 mol^{-1} yr^{-1}		f
k_{SFe3}	3.65×10^7	cm^3 mol^{-1} yr^{-1}	$10^2–10^8$	h,i,j
k_{Sviv}	1.0×10^7	cm^3 mol^{-1} yr^{-1}		
k_{SFeCO3}	1.0×10^7	cm^3 mol^{-1} yr^{-1}		
k_{FeSOx}	2.0×10^{10}	cm^3 mol^{-1} yr^{-1}	$10^8–10^{10}$	k,l
k_{FeSFe3}	0	g mol^{-1} yr^{-1}		
k_{FeSHS}	1.0×10^6	cm^3 mol^{-1} yr^{-1}	$10^6–10^{10}$	i,m
k_{surFe}	1.25×10^{10}	cm^3 mol^{-1} yr^{-1}		
k_{FeCO3}	4.5×10^{-4}	mol g^{-1} yr^{-1}		f
k'_{FeCO3}	0.25	yr^{-1}		f
K_{FeCO3}^r	4.0×10^{-15}	(mol cm^{-3})^2		
k_{viv}	1.7×10^{-9}	mol g^{-1} yr^{-1}		
k'_{viv}	1.0	yr^{-1}		
K_{viv}	3.0×10^{-50}	(mol cm^{-3})^5		n
k_{FeS}	4.0×10^{-5}	mol g^{-1} yr^{-1}	$10^{-7}–10^{-4}$	f,l
k'_{FeS}	1.0×10^{-3}	yr^{-1}		f
K_{FeS}	2.51×10^{-6}	mol cm^{-3}		o
K_{C1}	8.95×10^{-10}	mol cm^{-3}		
K_{C2}	5.22×10^{-13}	mol cm^{-3}		
K_{HS}	1.5×10^{-10}	mol cm^{-3}		
K_W	1.85×10^{-21}	(mol cm^{-3})^2		
K_{FeonFe}^*	4.5×10^{-3}	–		
K_{FeonB}^*	1.0×10^{-5}	–		
K_{PonFe}^*	6.0×10^{-2}	–		
K_{PonB}^*	1.0×10^{-5}	–		
$S_{TFe}(1-\gamma_{Fe})$	1.0×10^{-2}	mol g^{-1}		
$S_{TB}(1-\gamma_B)$	4.0×10^{-6}	mol g^{-1}		
D_b^0	10	cm^2 yr^{-1}	0.1–100	b

Interface concentrations (for solutes) and sedimentation fluxes (for solids) not listed in this table are zero.

*References: a) Roden and Edmonds (1997); b) Boudreau (1997); c) Hecky et al. (1993); d) Kalff (2002); e) Urban (1994); f) Van Cappellen and Wang (1996); g) Dittrich and coworkers, pers. commun., 2006; h) Wijsman et al. (2002); i) Fossing et al. (2004); j) Meysman et al. (2003); k) Van Cappellen and Wang (1995); l) Hunter et al. (1998); m) Rickard (1997); n) Davison (1993); o) Morse et al. (1987).

†Most natural unpolluted lakes have SO$_4$ concentrations in the lower part of the range (Urban, 1994).

account speciation of both phosphate ions and sorption sites leads to an expression similar to Eq. (6) but with a slightly smaller K_{adsP} for pH<7. The coefficients S_{Ti} $(1-\gamma_i)$ and $K_{P,i}^*$ for the Fe(III) substrate were obtained by fitting the experimental data of Parfitt (1989) for phosphate sorption on goethite (α-FeOOH). In our preliminary simulations, the choice of the sorption isotherm (e.g., Freundlich instead of Langmuir (Golterman, 1995)), had an insignificant effect on the magnitude of phosphorus efflux from the sediment.

3.3. Boundary conditions

The boundary conditions at the sediment–water interface are imposed-concentration (Dirichlet) for the dissolved species:

$$C_i(x=0,t) = C_i^0(t) \tag{7}$$

and imposed-flux (Neumann) for the solid species:

$$-\xi D_i \frac{\partial C_i}{\partial x} + \xi U C_i = F_i(t). \tag{8}$$

Here, F_i is the solid substance flux (in mol/cm^2-sed/yr) at the sediment–water interface. A no-gradient boundary condition is imposed for all species at the bottom of the integration domain (L = 10 cm):

$$C_i/\partial x|_{x=L} = 0. \tag{9}$$

In preliminary simulations, increasing L from 10 to 40 cm caused less than 2% variation in the phosphorus efflux from sediment and, thus, to increase the computation speed, L = 10 cm was chosen as the smallest realistic end-depth.

3.4. Coupling with the water column

Because up to 100% of the phosphorus deposited into the sediment can be released back into the water column (Emerson and Widmer, 1978) and then re-deposited in one form or another, a feedback exists between the phosphorus release and deposition fluxes. This may lead to a net accumulation in or a loss of phosphorus from the sediment. To take this "recycling" of phosphorus into account, we adopt a reflective boundary approximation (Soetaert et al., 2000) whereby phosphate flux from the sediment into the water column Φ_{out} (Fig. 1b) generates an equivalent amount in organic carbon rain flux $\Delta F_{OM} = \Phi_{rec}/z = \Phi_{out}/z$, where Φ_{rec} is the molar flux of the recycled phosphorus ($\Phi_{rec} = \Phi_{out}$ effectively assumes that the water-column biomass production is phosphorus-limited). Similarly, the dif-
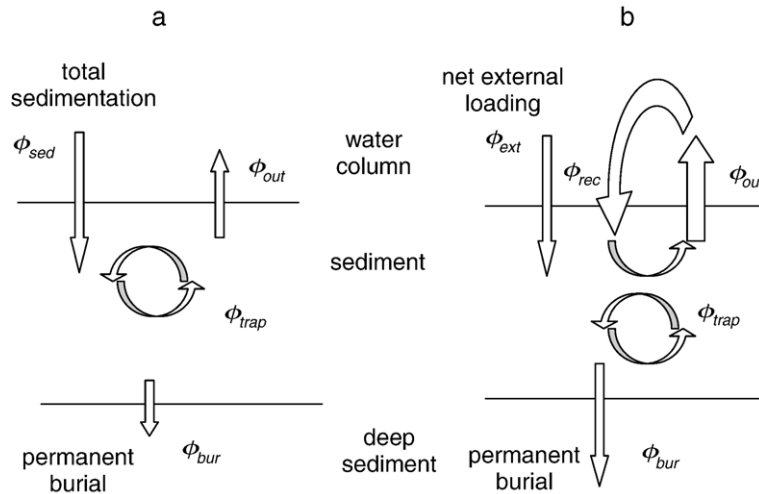
Fig. 1. Mass balance considerations and the recycling of phosphorus. a) No feedback between the sediment and the water column. Total sedimentation flux of phosphorus Φ_{sed} is specified as the model's boundary condition. In a steady-state, mass balance with the phosphorus burial flux Φ_{bur} demands that $\Phi_{out} = \Phi_{sed} - \Phi_{bur}$, irrespective of the internal fluxes Φ_{trap}. b) Phosphorus can be recycled in the water column, re-deposition flux $\Phi_{rec} = \Phi_{out}$. The boundary condition specifies the net external sedimentation flux Φ_{ext} (e.g., phosphorus input into the lake via rivers). The fluxes Φ_{rec} and Φ_{out} across the interface are not directly constrained by the mass balance between Φ_{ext} and Φ_{bur}. In a steady-state, $\Phi_{ext} = \Phi_{bur}$.

fusive efflux of Fe^{2+} is assumed to generate its molar equivalent in the sedimentation flux of ferric iron $F_{Fe(OH)3}$, i.e. all dissolved ferrous iron is oxidized in the water column (Fossing et al., 2004). The reflective boundary approximation is appropriate for the steady-state calculations in this paper. Simulating temporal evolution of diagenetic systems may require additional water-column variables (Soetaert et al., 2000) to account for the time delay between the release of sediment substances and their re-deposition.

We perform our simulations for two situations: without the recycling of phosphorus and iron, in which case total sedimentation fluxes Φ_{sed} are specified at the model boundary (see Fig. 1a), and with such recycling, in which case only net external fluxes Φ_{ext} are specified (see Fig. 1b).

3.5. Numerical method

Nonlinear coupled partial differential Eq. (1) with boundary conditions (7–9) was discretized on an evenly spaced grid so that the species concentrations at each node were described by a system of ordinary differential equations (ODE). The resulting ODEs were solved with a method-of-lines stiff ODE integrator VODE (Brown et al., 1989) to obtain the species concentrations $C_i(x,t)^-$. Steady-state solutions $C_{st}(x)$ were obtained by running the program for diagenesis times sufficiently long for any transient behaviors to vanish, 10,000 years in our simulations. Total analytical variables ([TC], [TS], and

[ALK], respectively) were used to characterize the aqueous concentrations of porewater carbonate, sulfide, and alkalinity:

$$[TC] = [CO_2] + [HCO_3^-] + [CO_3^{2-}], \tag{10}$$

$$[TS] = [HS^-] + [H_2S], \tag{11}$$

$$\begin{aligned}[ALK] = &\;[HCO_3^-] + 2[CO_3^{2-}] + [HS^-] - [NH_4^+] \\ &+ F[ads - Fe] - [H^+] + [OH^-].\end{aligned} \tag{12}$$

We assumed that the adsorption reactions are in local chemical equilibrium so that the amounts of ferrous iron and phosphate can be expressed as total (dissolved + adsorbed) quantities:

$$\begin{aligned}[totFe] &= [Fe^{2+}] + [ads - Fe]F \\ &= [Fe^{2+}](1 + FK_{adsFe}),\end{aligned} \tag{13}$$

$$\begin{aligned}[totP] &= [P_{diss}] + [ads - P]F \\ &= [P_{diss}](1 + FK_{adsP}),\end{aligned} \tag{14}$$

The conversion factor F between the concentration units for solid and liquid species is $F = \rho(1 - \varphi)/\varphi$. The term $F[ads-Fe]$ in the expression for total alkalinity [ALK] (Eq. (12)) accounts for the release of H^+ in the Fe^{2+} sorption/desorption reaction 18 (Table 1).

Since the adsorption coefficients (4) and (6) depend on the proton concentration $[H^+]$, which, in turn, cannot be determined independently of [ads-Fe] (because both [ads-Fe] and $[H^+]$ enter Eq. (12)), a Newton–Raphson algorithm was employed to determine the concentrations

$[Fe^{2+}]$ and $[H^+]$ at each iteration step by simultaneously solving Eqs. (12) and (13) with known [ALK] and [tot-Fe], together with Eq. (4) and the equilibrium relations in Table 1. Concentrations of all other equilibrium species were calculated from the equilibrium speciation relations in Table 1 and the sorption relations (3–6).

3.6. Omitted processes

We keep the number of processes in the model to a minimum that still reflects the essential features of the classical model and the sulfate-induced phosphorus mobilization. As such, we ignored phosphorus immobilization with apatite (Golterman, 2001) and aluminum (Williams et al., 1971), and complexation of iron, sulfur, and phosphorus with sediment organic matter (Jackson and Schindler, 1975), as well as redox-sensitive uptake and release of phosphorus by benthic bacteria (Gächter et al., 1988). We neglected phosphorus immobilization with $CaCO_3$ (House et al., 1986) because of the low calcite concentration at the circumneutral pH considered here. Phosphorus loading to the sediment surface is considered only with organic matter, without explicit treatment of other sources such as fertilizer pollution (runoff) and mineral phosphorus input. Sediment nitrogen and manganese are not considered, for simplicity. In preliminary simulations (not shown), nitrogen and manganese decreased phosphorus efflux by shifting the iron reduction zone to deeper sediment but their presence was inconsequential for the main conclusions of this paper.

As is often done in RTMs (e.g., Boudreau, 1996), we disregarded sediment heterogeneity and finite grain size. Also, the functional form of the mineral precipitation rate laws in Table 2 is consistent with mineral formation by nucleation, ignoring crystal growth and ripening. Aqueous solutions are assumed ideal so that activities are replaced by concentrations.

We also had to exclude bio-irrigation (pumping activity by burrow-dwelling animals which results in a non-local fluid exchange between porewater and bottom water) from factorial simulation runs because numerical difficulties in many of such runs precluded a complete factorial analysis.

4. Factor analysis design

We determine phosphorus control parameters by performing both local and global sensitivity analyses on our model. In the local sensitivity analysis, model behaviors are simulated in response to small deviations in the model parameters (such as reaction rate constants

or reactive species input fluxes) from a selected point in the model parameter space. In diagenetic RTM studies (e.g., Van Cappellen and Wang, 1996a), such a point is typically defined by a parameter set for which a satisfactory fit to the data is obtained. Model sensitivity is typically expressed in terms of derivatives $\frac{\partial y_i}{\partial \theta_j}$, where y_i are the response functions (e.g., calculated values of model variables) and θ_j are model parameters. To compare the effects of different parameters, the derivatives are scaled as $\frac{\partial y_i}{\partial \theta_j}\Delta\theta_j$ (to express them in units of y_i) or $\frac{\partial y_i}{\partial \theta_j}\Delta\theta_j/y_i^{sc}$, (in dimensionless units), where y_i^{sc} are the characteristic scales for the variables y_i. The parameters $\Delta\theta_j$ can reflect, for example, the constraints (ranges) or uncertainties in the respective θ_j values imposed by the available field data or prior knowledge. However, the choice of both y_i^{sc} and $\Delta\theta_j$ is subjective, and this can affect the analysis results (Brun et al., 2001). To eliminate the bias associated with $\Delta\theta_j$, we choose $\Delta\theta_j = \theta_j$ so that the scaled derivatives become relative deviations, i.e. the percent change in y_i given the percent change in θ_j (Omlin et al., 2001). In performing local sensitivity analysis, we investigate our model behavior around a single point in the model parameter space defined by the parameter set in Table 3 representative of the typical lake sediment conditions.

Global sensitivity analysis involves investigating a larger region of the model parameter space (Hornberger and Spear, 1981; Elliott et al., 2000; Brun et al., 2001). We utilize a so-called 2^k factorial design setup (Montgomery, 1997; Saltelli et al., 2000) whereby model solutions are obtained for two levels (maximum and minimum) of k selected parameters, as described below. While less computationally efficient than some other parameter screening methods (Morris, 1991; Reichert et al., 2002), this approach has the advantage of estimating parameter interactions, i.e. to what degree the effect of varying one model parameter depends on the values of the others. In a complex and interconnected diagenetic system, this is important because, as demonstrated below, phosphorus control factors may vary with sediment conditions. The minimum and maximum parameter levels (Table 4) were selected to bracket the typical or expected variability ranges for the respective parameters. Because of an inherent freedom in the choice of those levels, and because parameters such as reaction rate constants can vary by as much as several orders of magnitude, the analysis identified factors that are potential phosphorus controls when varied across this selected range of possible conditions, rather than at a particular system or site. The parameter ranges were determined by searching the literature for typical species concentrations and

Table 4
Parameter selection for 2^k factorial analysis

Parameter	Group								Min. value	Max. value	Unit
	A	B	C	D	E	F	G	H			
F_{OM}						x			1.25×10^{-3}	5.0×10^{-3}	mol cm^{-2} yr^{-1}
$F_{Fe(OH)3}$	x	x	x			x			1.25×10^{-5}	7.0×10^{-5}	mol cm^{-2} yr^{-1}
$[O_2]^0$		x			x	x		x	0	1.5×10^{-7}	mol cm^{-3}
$[SO_4]^0$	x	x	x			x			1.0×10^{-8}	0.5×10^{-6}	mol cm^{-3}
k_{OM}						x			0.3	0.9	yr^{-1}
k_{FeSFe3}		x	x				x		0	1.0×10^{4}	g mol^{-1} yr^{-1}
k_{SFe3}			x				x		3.0×10^{2}	3.0×10^{8}	cm^3 mol^{-1} yr^{-1}
k_{Sviv}	x				x			x	0	1.0×10^{8}	cm^3 mol^{-1} yr^{-1}
k_{SFeCO3}	x								0	1.0×10^{8}	cm^3 mol^{-1} yr^{-1}
k_{FeSOx}							x	x	3.0×10^{8}	2.0×10^{10}	cm^3 mol^{-1} yr^{-1}
k_{FeSHS}				x	x		x		0	1.0×10^{10}	cm^3 mol^{-1} yr^{-1}
k_{FeS}								x	4×10^{-7}	4×10^{-4}	mol g^{-1} yr^{-1}
k_{viv}	x			x	x			x	1.0×10^{-10}	3.0×10^{-9}	mol g^{-1} yr^{-1}
k'_{viv}	x								0.1	10	yr^{-1}
D_b^0		x			x				1	10	cm^2 yr^{-1}
τ				x					2	5	cm
U				x	x				0.1	0.3	cm yr^{-1}
K^*_{FeonFe}			x						5.0×10^{-4}	1.0×10^{-2}	–
K^*_{FeonB}			x						5.0×10^{-6}	5.0×10^{-5}	–
K^*_{PonFe}		x		x					2.0×10^{-2}	1.0×10^{-1}	–
K^*_{PonB}				x					5.0×10^{-6}	5.0×10^{-5}	–

Factors included in each factor group are marked by 'x'.

polling the dSED database (Katsev et al., 2004) for typical ranges of kinetic constants.

The effects of individual model parameters and their interactions were calculated as differences between the response function values corresponding to the maximum and minimum levels of the selected factor(s), averaged over all levels of all other factors (Montgomery, 1997). For example, for a simple two-factor analysis (Fig. 2), the effects E_A and E_B of individual parameters A and B on the response function Y are:

$$E_A = 0.5[Y_{ab} + Y_a - Y_b - Y_{(1)}] = <Y>_{A+} - <Y>_{A-} \tag{15}$$

$$E_B = 0.5[Y_{ab} + Y_b - Y_a - Y_{(1)}] = <Y>_{B+} - <Y>_{B-} \tag{16}$$

where Y_i are the response function values at the respective points in the A–B parameter space (Fig. 2) and $<Y>_+$ and $<Y>_-$ are the averages of the response function for the maximum and minimum levels of the respective parameter over all levels of the other parameter.

The interaction E_{AB} between the factors A and B is defined as:

$$E_{AB} = 0.5[(Y_{ab} - Y_b) - (Y_a - Y_{(1)})], \tag{17}$$

i.e. the difference in the effects of A (or B) between the maximum and minimum levels of B (or A). More details can be found in the factorial analysis literature (e.g., Montgomery, 1997).

Characterizing the response function by its values at only two parameter levels implicitly assumes that the system response is approximately linear within the considered parameter range (the validity of this assumption can be verified by analyzing the distribution of standardized residuals, which are the deviations of individual response function values from their average). Given the calculated response function values, the response function can be approximated with a linear regression

$$Y = a_0 + \sum_i a_i x_i + \sum_{j\neq i} a_{ij} x_i x_j + \varepsilon, \tag{18}$$

where x_i are the values of the model factors scaled linearly so that $+1$ corresponds to the maximum factor level and -1 corresponds to the minimum factor level (Table 4). The term å denotes the higher-order terms and terms proportional to x_i^2 that are neglected. The regression coefficients a_0, a_i and a_{ij} are calculated to fit the calculated response function values (Montgomery, 1997).

For the sake of simplicity, we choose a single response function: The steady-state diffusive phosphorus
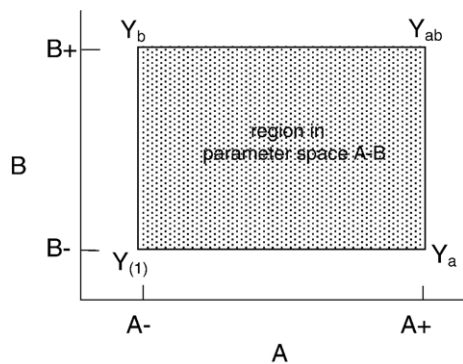
Fig. 2. Global sensitivity analysis in a 2^k factorial design. For a two-parameter analysis, the response function Y is calculated at four points ((1), a, b, and ab) corresponding to the 2^2 combinations of the maximum (+) and minimum (−) levels of factors A and B.

efflux Φ_{out} from the sediment into the water column (Fig. 1). The steady-state approximation allows the comparison of time-independent quantities instead of dynamic solutions, i.e. numbers instead of functions. It also avoids time-dependent inputs to the model, such as temporal variations in the sediment temperature or hypolimnetic oxygen concentration. The use of the steady-state approximation in lake sediments where phosphorus fluxes fluctuate daily (Carlton and Wetzel, 1988), seasonally (Søndergaard et al., 2001), and over many years (Gächter and Müller, 2003) restricts the analysis to time scales that are greater than the typical relaxation times in a diagenetic system, i.e. the analysis identifies parameters that determine the long-term trends in phosphorus efflux. The system evolutions on time scales greater than the typical transition times between steady-states (e.g., after a change in external conditions) can be described by a succession of steady-states. The steady-state solutions can also be interpreted as the time-averages of the system characteristics (Soetaert et al., 1996).

5. Results and discussion

5.1. Typical solutions

In the absence of phosphorus and iron recycling in the water column (Fig. 1a), phosphorus efflux from sediment Φ_{out} typically approached its steady-state value within 10 to 20 years in our simulations (Fig. 3). (The results for the boundary condition which takes P and Fe recycling into consideration (Fig. 1b) will be discussed later.)

Because chemical species distributions within natural lake sediments exhibit extremely large lateral (from cm to km) and temporal (diurnal to seasonal to inter-annual) variability (e.g., Lewandowski et al., 2002), depth

profiles determined by measurements in situ do not, in general, coincide with their respective long-term and/or large-scale averages. Because steady-state model solutions here effectively represent such averages, we chose not to calibrate our model to a particular single set of field data but instead selected a reference state (Table 3) variations about which generated depth profiles that are consistent, in terms of the species concentrations and profile shapes, with a large number of field observations (e.g., Rudd et al., 1986; Fürrer and Wehrli, 1996; Lewandowski et al., 2002, and other works). Fig. 4 illustrates such typical simulated steady-state depth profiles and Table 5 compares typical freshwater sediment characteristics with their simulated values corresponding to the parameter set in Table 3.

Because of equilibration with the water column where high biological demand is considered to consume all inorganic phosphate (phosphorus limitation of biological production), the concentrations of both dissolved [P_{diss}] and adsorbed [ads-P] phosphate reach zero at the sediment–water interface (Fig. 4). Porewater phosphate concentration is small within the oxic layer (x=0–3 mm) where phosphate is sorbed to solid Fe(III) and increases below 3 mm because of the phosphate production from decomposing organic matter (reactions 1–4 in Table 1). The [ads-P] profiles often have double maxima that arise in the absence of temporal changes in phosphorus deposition as a combined effect of several factors: the in-sediment phosphate production, the microbial iron reduction which decreases the amount of Fe(III) sorption substrates with depth, and the porewater pH variation with depth. Microbial iron and sulfate reduction causes the porewater concentrations
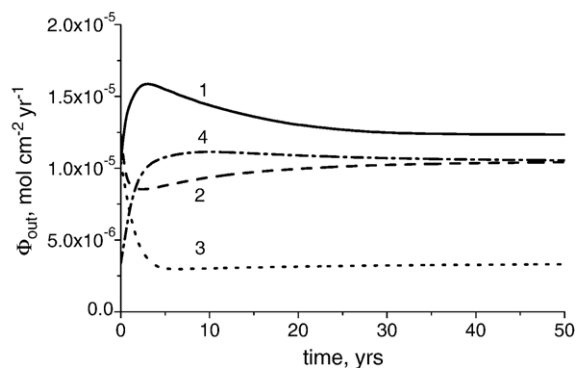

Fig. 3. Approach to a steady-state. Time evolution of the phosphorus efflux from sediment Φ_{out} is plotted after the system is perturbed from a steady-state as follows. 1)[O_2]^0 is switched from 0.1 to 0.005 mM. 2) [O_2]^0 is switched from 0.005 to 0.1 mM. 3) F_{OM} is halved from its value in Table 3. 4) F_{OM} is restored (doubled from its value in case (3)). There is no feedback between the sediment and the water column (Fig. 1a).
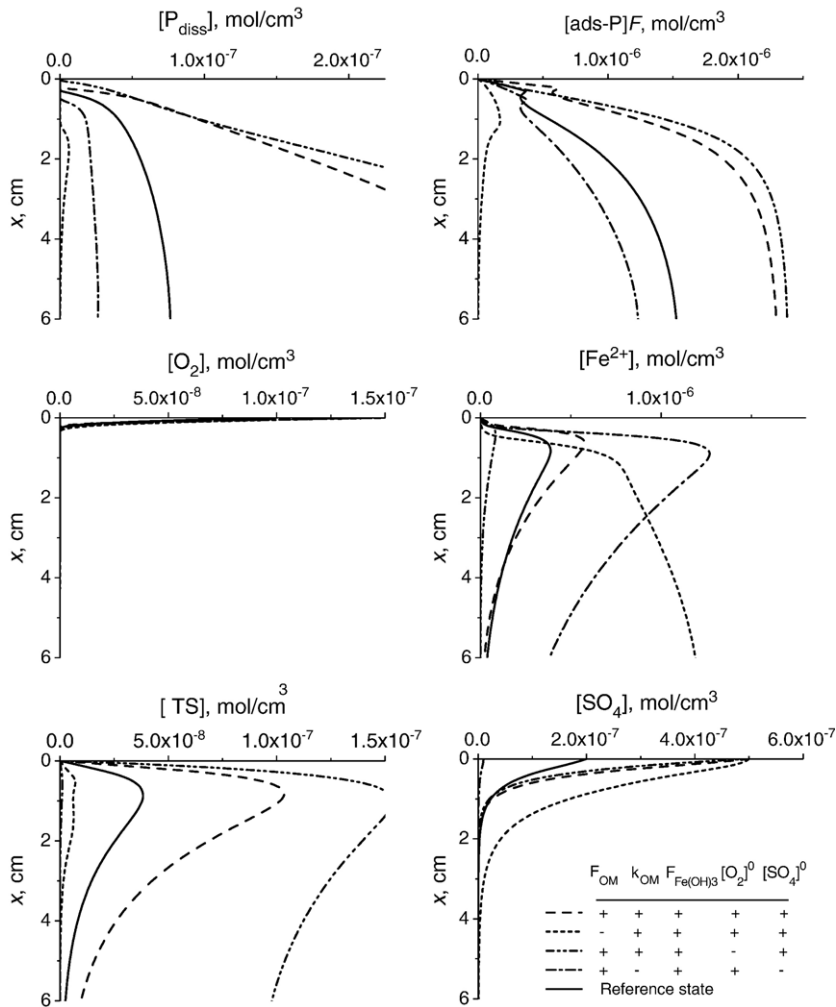
Fig. 4. Simulated steady-state depth profiles. The solid lines correspond to the parameter set in Table 3 (reference state). For other curves, the parameters marked "−" in the legend are at their minimum levels (see Table 4), and the ones marked "+" are at their maximum levels, while all other parameters are as in Table 3.

$[Fe^{2+}]$ and [TS] to increase with depth, but both these concentrations decrease in the deeper sediment because of the precipitation of iron sulfide, FeS, and vivianite. The sulfate reduction and the associated presence of hydrogen sulfide immediately below the interface are consistent with the porewater profiles for the respective species observed in lakes (Postma and Jakobsen, 1996; Alfaro-De la Torre and Tessier, 2002) and the recently reported high densities of sulfate reducers in sediment oxic zones (Wieringa et al., 2000).

5.2. Control parameters for steady-state P efflux

5.2.1. Individual factor effects

The results of local and global factor analyses are summarized in Fig. 5. For the local analysis, relative (percentage) deviations from the reference Φ_{out} value were calculated in response to increasing the respective model parameter values by 1%. To perform the global sensitivity analysis, the number of simulation runs was reduced to a manageable size by distributing the model parameters in groups (typically 6 parameters per group). For each group, steady-state effluxes of phosphorus Φ_{out} were calculated for all $2^6 = 64$ combinations of parameter (factor) levels in a group (Table 4).

As seen in Fig. 5, the sedimentation flux of organic matter F_{OM} is the most important factor in determining the magnitude of the steady-state phosphorus flux across the sediment–water interface. Variations in F_{OM} generate changes in Φ_{out} that exceed the direct production of phosphorus from OM by a factor of about 1.5. Other significant parameters include $[O_2]^0$, $[SO_4]^0$, and F_{Fe}

Table 5
Simulated steady-state sediment characteristics for the parameter set in Table 3

Characteristic	Value for $F_{OM}=\Phi_{sed}/z$ (oxic/anoxic [a])	Value for $F_{OM}=\Phi_{ext}/z$ (oxic/anoxic [a])	Units	Typical value	Ref.
Efflux Φ_{out}	$(1.0/1.2)\times10^{-5}$	$(0.8/13)\times10^{-5}$	mol/cm^2/yr	$(1–6)\times10^{-5}$ [b]	1,5
$[OM]^0$	1.8×10^{-3}	$(1.3/18)\times10^{-3}$	mol/g $_{DW}$	$(1.5–9)\times10^{-3}$ [c]	
$[Fe(OH)_3]^0$	$(9/1.3)\times10^{-6}$	$(9/1.8)\times10^{-6}$	mol/g $_{DW}$	$(1–2.5)\times10^{-4}$ [d]	11
$[Fe_3(PO_4)_2]$ [e]	$(8/0.5)\times10^{-6}$	$(7/0.7)\times10^{-6}$	mol/g $_{DW}$	$0–10^{-5}$	12,13
tot Fe in solid [e]	$(3/0.16)\times10^{-5}$	$(2.5/1)\times10^{-5}$	mol/g $_{DW}$	$(0.1–2)\times10^{-3d}$	2,6,9
tot P in solid [e]	$(15/4)\times10^{-6}$	$(15/5)\times10^{-6}$	mol/g $_{DW}$	$(3–20)\times10^{-5}$	2
Fe:P in solid [e]	$(1.5–2.3)/(7–20)$	$(1.7–2.4)/(1.3–3.7)$	–	$2–10$ [d]	2,6,14
$[TS]$ [e]	$(2.0/3.5)\times10^{-8}$	$(2.0/5)\times10^{-8}$	mol/cm^3	1×10^{-8}	10
S reduction rate [f]	$(5/8)\times10^{-5}$	$(4/)\times10^{-5}$	mol/cm^2/yr	$(0.3–50)\times10^{-5}$	7
$[P_{diss}]$ [e]	$(6/15)\times10^{-8}$	$(4/200)\times10^{-8}$	mol/cm^3	$(2–20)\times10^{-8}$	3,4
$[Fe^{2+}]$ [e]	$(20/2.5)\times10^{-8}$	$(20/2.5)\times10^{-8}$	mol/cm^3	$(2–50)\times10^{-8}$	3,4,6
FK_{adsP} [g]	2000/150	2000/150	–	$2–1000$	2
pH at interface	7.2	7.2	–	$4–9$	

References: 1) Boström et al. (1988); 2) Jensen et al. (1992); 3) Carignan and Lean (1991); 4) Fürrer and Wehrli (1996); 5) Kalff (2002); 6) Roden and Edmonds (1997); 7) Urban (1994); 8); 9) Carignan and Tessier (1988); 10) Wersin et al. (1991); 11) Kliza and Telmer (2001); 12) Manning et al. (1991); 13) Emerson and Widmer (1978); 14) Hupfer et al. (1995).

[a] Values for anoxic sediment are obtained by setting $[O_2]^0=0$ for fixed Φ_{sed} and $[O_2]^0=10$ μM for fixed Φ_{ext}.

[b] From anoxic sediments during summer anoxia for periods from days to months.

[c] Sediment organic content varies in a wide range between environments. The typical value here was calculated by assuming 5–30% DW organic content and OM molar mass 30 g/mol.

[d] Includes both reactive and refractory Fe(III) fractions.

[e] Average over the upper 10 cm of sediment.

[f] Integrated over the upper 10 cm of sediment.

[g] Within the top 2 cm of the sediment.

$_{(OH)3}$, whose individual effects are roughly comparable in magnitude, both in local and global analyses. Φ_{out} also strongly depends on the organic matter reactivity (k_{OM}) and the sedimentation (burial) rate U, as well as on the rate of phosphate immobilization with ferrous phases (effectively described by k_{viv}) and on the rate of dissolution of those phases by porewater hydrogen sulfide (described by k_{Sviv}). The following parameters had negligible effects on Φ_{out}: bioturbation intensity D_b^0, the rates of dissolution of Fe(OH)$_3$ and FeCO$_3$ by hydrogen sulfide (represented by k_{SFe3} and k_{SFeCO3}, respectively), the rate of FeS precipitation (k_{FeS}), and the sorption of phosphate and dissolved iron on both types of substrates (represented by the respective K_i^* constants). Changing the porewater pH at the sediment–water interface (by varying the alkalinity variable $[ALK]^0$ while maintaining constant $[TC]^0$) in the range from 6 to 8 did not significantly affect Φ_{out}.

To test the effect of sediment temperature on Φ_{out}, the molecular diffusion coefficients were re-calculated for $T=15$ °C and the reaction rate constants were corrected for temperature using the Arrhenius law with a Q_{10} factor (a factor by which the parameters increase per 10 °C) of 2. The bioturbation coefficient D_b^0 was temperature-corrected using $Q_{10}=3$ (c.f. Fossing et al., 2004). It was found that the phosphorus efflux Φ_{out} at $T=15$ °C differed from its value at $T=5$ °C by less than 15%, which is comparable to the minor factor effects in Fig. 5.

5.2.2. Factor interactions

Several two- and three-factor interaction effects are comparable in magnitude with the individual factor effects (Fig. 5), which indicates that, for the parameter ranges considered, phosphorus efflux from sediment is determined by the balance, rather than absolute values, of the respective sediment characteristics: organic matter flux F_{OM}, the interface concentrations of oxygen $[O_2]^0$ and sulfate $[SO_4]^0$, and the sedimentation flux of ferric iron $F_{Fe(OH)3}$.

These interactions are illustrated in Fig. 6 as contour plots of the Φ_{out} values calculated from a linear regression of the type shown in Eq. (18). The approximately straight contour lines in the plots $[O_2]^0$ vs. F_{OM} and $[SO_4]^0$ vs. F_{OM} (Fig. 6a,b) suggest that the large values of the corresponding interaction effects in Fig. 5 are mainly due to the strong effect of the organic matter flux F_{OM}. In contrast, curved contour lines in Fig. 6c–d indicate a significant interdependence between the effects on the phosphorus efflux of the interface concentrations $[O_2]^0$ and $[SO_4^{2-}]^0$, and the sedimentation
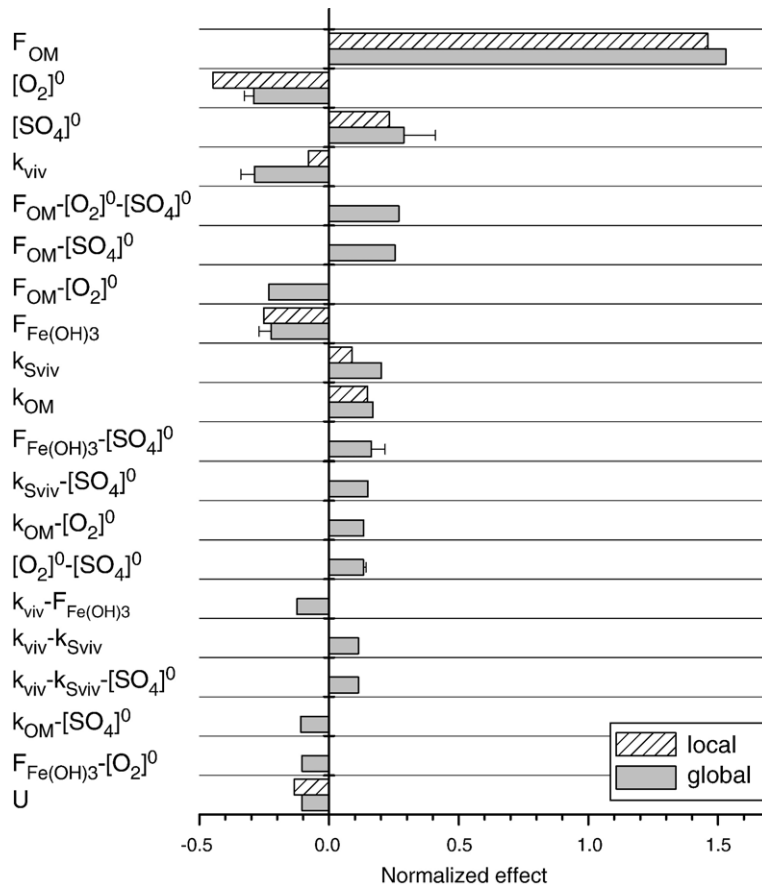
Fig. 5. Sensitivity analyses summary. Local sensitivity analysis (relative deviation): the percent change in Φ_{out} in response to varying individual parameters by 1%. Global sensitivity (2^k factorial) analysis: The magnitudes of the most significant factor and interaction effects normalized by the reference Φ_{out} value. The error bars correspond to a standard deviation over the factor groups (Table 4). Positive (negative) effects indicate that an increase in the respective parameter increases (decreases) P efflux from the sediment. The model boundary condition at the sediment–water interface specified Φ_{sed} (Fig. 1a).

flux of ferric iron $F_{Fe(OH)3}$. Fig. 7 shows Φ_{out} values calculated from the model for a range of these parameters.

The correlations between the diagenetic effects of $F_{Fe(OH)3}$, $[O_2]^0$, and $[SO_4]^0$ on phosphorus mobilization are realized via a number of reactive pathways, as determined by an inspection of the simulated depth profiles and by running simulations with one or several parameters selectively turned off. For example, FeS precipitation affects porewater concentrations of both Fe^{2+} and H_2S. Whereas increasing the supply of iron $F_{Fe(OH)3}$ to the sediment may increase phosphorus immobilization with vivianite, it can be compensated by an appropriate increase in $[SO_4]^0$, which generates H_2S that binds Fe(II), thereby limiting the sediment vivianite content. Because the dissolved sulfate affects phosphorus efflux via the diagenetic cycle of iron, the effect of sulfate on Φ_{out} is greater in Fe-rich sediments (Fig. 7).

Similarly, the effect of sulfate is greater at higher oxygen concentrations, because of the larger Fe^{2+} concentration below the oxic layer. Conversely, varying $[O_2]^0$ has a smaller effect on Φ_{out} at high sulfate concentrations because of the low dissolved Fe^{2+} amounts in reduced sediment. Oxidation of H_2S and FeS by oxygen (reactions 7 and 8 in Table 1) did not affect either Φ_{out} or the magnitude of the $[O_2]^0$–$[SO_4]^0$ interaction in our simulations.

To verify consistency with the local sensitivity analysis in the limit of small deviations, a separate factorial analysis was performed with the minimum and maximum parameter levels assigned as the reference value in Table 3 plus or minus 1%, respectively. The individual factor effects in this analysis coincided with their corresponding values in the local analysis, whereas interactions between factors were negligible. The latter result indicates relative independence of the factor
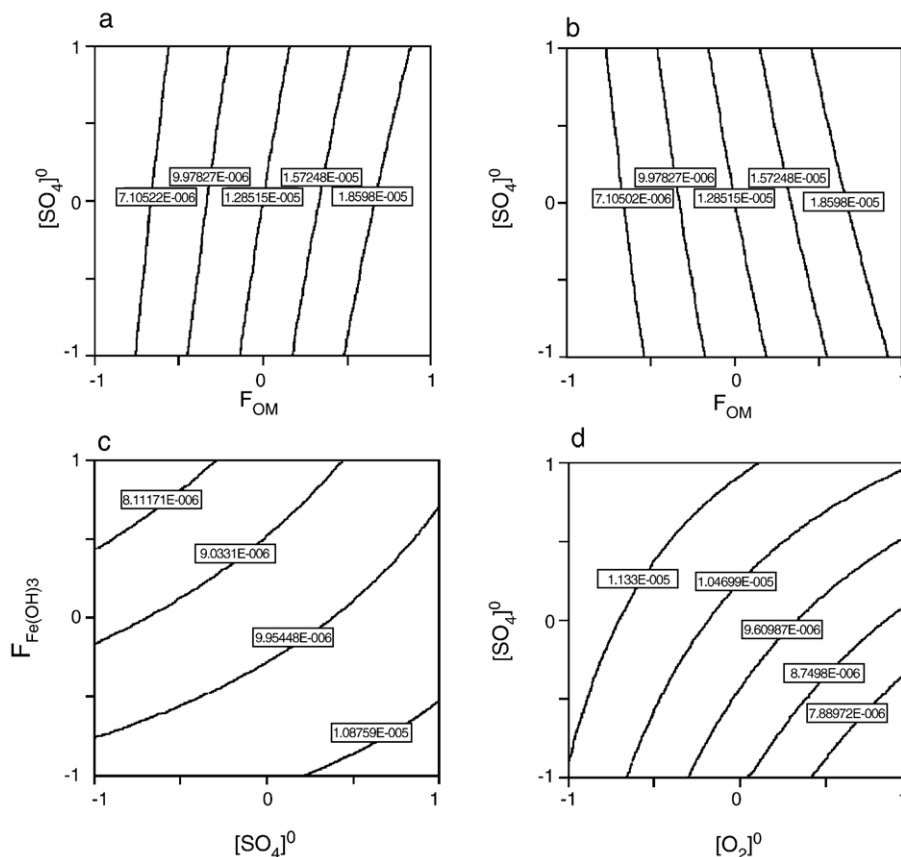
Fig. 6. The most significant parameter interaction effects. The values of Φ_{out} (in mol/cm^2/yr) are calculated from linear regression (Eq. (18)) using the data of 2^k factorial analysis and are constant along the contour lines. The axes are linearly scaled for convenience so that -1 and $+1$ correspond to the minimum and maximum values of the plotted factor (Table 4).

effects for small deviations around the reference state, which is also manifested in the small variation in the line curvature in the central regions of Figs. 6 and 7.

5.3. Short-term vs. long-term phosphorus efflux

In an apparent contradiction with the classical model, the list of phosphorus control factors in Fig. 5 does not include model parameters that define phosphorus immobilization near the sediment surface, such as constants K^*_{PonFe} and k_{SFe3} that characterize the strength of phosphate sorption to Fe(III) oxyhydroxides and the rate of Fe(III) dissolution by H_2S, respectively. This contradiction illustrates an important distinction between phosphorus controls in a long-term (e.g., decades) and on short time scales for which the classical model was originally formulated (days to months) (Mortimer, 1941).

Long-term phosphorus retention can be summarized by a simple mass balance argument (see Fig. 1): Phosphorus that is not buried has to be released. For a constant phosphorus input rate Φ_{sed}, the steady-state efflux of phosphorus into the water column Φ_{out} is linked to the permanent burial flux Φ_{bur} so that $\Phi_{out} = \Phi_{sed} - \Phi_{bur}$ (Fig. 1a). In order to increase long-term retention of phosphorus, any immobilization of phosphorus within the diagenetically active sediment layer (including phosphorus sorption to iron oxyhydroxides in the oxidized layer) has to be accompanied by its permanent burial. For instance, phosphorus sorption to Fe(III) near the sediment interface may indirectly increase the rate of vivianite precipitation in deep sediment by increasing the time that phosphorus spends in the diagenetically active layer. In case phosphorus is mobilized before it is permanently buried (e.g., because of the dissolution of Fe(III) sorption substrates), phosphorus immobilization near the sediment surface is ineffective for its long-term retention (Hupfer et al., 1995). Phosphorus will accumulate inside the sediment and eventually will be released to the overlying water. In the short-term, however, the mass balance between the input and burial fluxes can be (temporarily) violated and
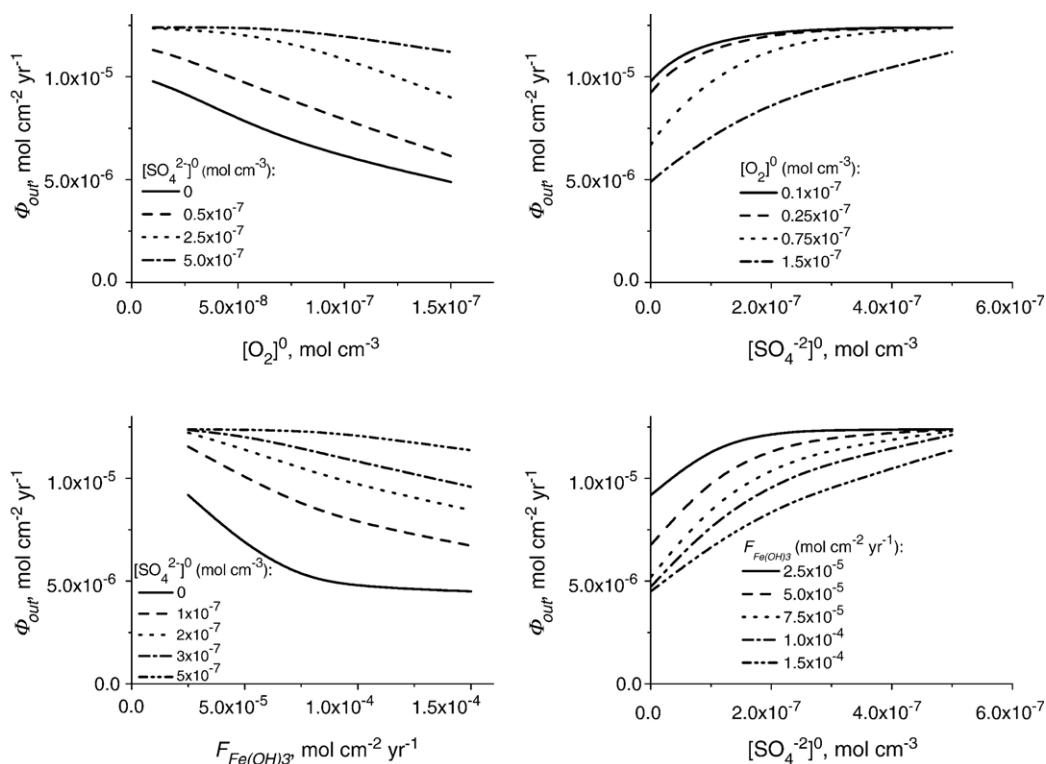
Fig. 7. The effects of $[O_2]^0$, $[SO_4]^0$, and $F_{Fe(OH)3}$ on the steady-state value of phosphorus efflux Φ_{out}. The sedimentation flux of phosphorus at the model's boundary Φ_{sed} was 1.285×10^{-5} molP/cm^2/yr. The non-varied parameters are as in Table 3.

sediment phosphorus exchange with the water column can be dominated exclusively by the processes near the sediment–water interface. This difference between long-term and short-term phosphorus retention mechanisms means that the mechanisms for seasonal phosphorus releases can be different from the ones that control phosphorus accumulation or removal over the time span of decades.

That phosphorus release mechanisms depend on the time scale of interest has been a source of a considerable amount of confusion. For example, short-term laboratory and in-situ observations (e.g., Mortimer, 1941) that phosphorus effluxes are restricted by higher bottom water oxygen concentrations were used as a rationale in long-term lake management projects (Gächter and Wehrli, 1998). Our results show that even though higher oxygen concentration in the bottom water can improve the long-term phosphorus retention (Fig. 7) (c.f. Schauser et al., 2006), the mechanisms are different from those in the classical model and thus lake restoration by hypolimneon oxygenation may not have the desired long-term effect (Gächter and Wehrli, 1998; Gächter and Müller, 2003; Schauser et al., 2003).

In our simulations, for sufficiently low sulfate concentration, the presence of oxygen at the sediment surface increases the concentration of dissolved iron $[Fe^{2+}]$ below the oxic layer through Fe^{2+} oxidation and sorption to ferric oxyhydroxides (reactions 5, 6, and 18 in Table 1), thus preventing the loss of iron to the water column. As ferric oxyhydroxides are buried into the reduced sediment, they are reductively dissolved and Fe^{2+} and H_3PO_4 are released to the porewater in the deeper part of the sediment. Increasing $[O_2]^0$ or $F_{Fe(OH)3}$ raises the porewater supersaturation with respect to vivianite below the oxic zone and thus enhances phosphorus burial. In addition, a higher concentration of oxygen increases the supersaturation with respect to vivianite by shifting the iron reduction zone and its associated Fe^{2+} concentration maximum deeper towards the maximum in the concentration of dissolved phosphate. The strength of phosphorus sorption near the sediment surface was unimportant for Φ_{out} in our simulations and the curves in Fig. 7 were virtually unchanged when the adsorption of phosphate on $Fe(OH)_3$ was turned off in the model by setting $K^*_{PonFe}=0$.

Given the importance of permanent phosphorus burial, more research is needed to experimentally characterize phosphorus-bearing solid phases with which phosphorus is permanently buried in natural sediments. Their amounts and mineralogy, as well as the

kinetics of their formation and dissolution (such as the processes described here by the kinetic constants k_{viv}, k'_{viv}, and k_{Sviv}) need to be determined. For example, sediment porewaters are often found to be supersaturated with respect to vivianite (Emerson and Widmer, 1978; Wersin et al., 1991; Friedl et al., 1997) but substantial vivianite quantities are rarely reported (Nriagu and Dell, 1974; Manning et al., 1991, 1999). Some authors suggested that vivianite precipitation is typically inhibited or very slow (e.g., Wersin et al., 1991). Alternatively, amorphous or nanophase particles of vivianite-like iron phosphates could fall below the detection limits of experimental techniques. Ferrous phosphate agglomerates (e.g., $Fe(OH)_2$–PO_4) on the surfaces of solid particles (Roden and Edmonds, 1997) could also contribute to permanent phosphorus burial.

In characterizing phosphorus-bearing phases, it is important to distinguish adsorbed phosphorus from phosphorus in authigenically precipitated minerals (Golterman, 1995). Mineral precipitation limits the porewater phosphate amount to near-equilibrium concentration; adsorption, on the other hand, only redistributes phosphorus between solid and liquid phases and thus dissolved phosphorus concentration may increase with phosphorus input to the sediment.

5.4. Recycling in the water column and re-deposition

The mass balance considerations in the previous section (Fig. 1a) need to be modified if water-column recycling of the released sediment material is substantial (Fig. 1b). Assuming 100% recycling efficiency (in a steady-state, $\Phi_{out}=\Phi_{rec}$), the steady-state burial flux Φ_{bur} has to be equal to the net external input flux of phosphorus Φ_{ext}, which is the difference between the phosphorus amounts delivered to and flushed from the lake by rivers and other inputs and outputs (e.g., aerosols, ground water, run-off). In this case, Φ_{ext} and Φ_{bur} impose no direct mass balance constraints on the magnitude of Φ_{out} ($=\Phi_{rec}$), and Φ_{out} can be controlled by the near-interface processes. However, physical transport of substances by diffusion and bioturbation creates feedbacks between phosphorus diagenesis at different depths within the sediment, providing an indirect link between Φ_{bur} and Φ_{out}. The burial flux Φ_{bur} is determined by the rate of phosphorus-bearing solids formation (within the cycle Φ_{trap}), which, in turn, is affected by the porewater phosphate and iron concentrations, which are themselves affected by the amounts of phosphorus and iron cycling across the sediment–water interface (cycle Φ_{out}–Φ_{rec}). Over time, the Φ_{out}–Φ_{rec} cycle has to adjust so that $\Phi_{bur}=\Phi_{ext}$. Thus,

the long-term phosphorus efflux Φ_{out} is determined not only by near-interface processes but also by phosphorus cycling in the deeper sediment (Φ_{trap}) and by permanent P burial processes (Φ_{bur}).

Fig. 8 plots transient efflux Φ_{out} for the case where the released phosphorus and iron are rapidly (the re-deposition time is much shorter than the characteristic system evolution time scale) recycled back to the sediment. Because of the complexity of the feedback interactions between the input and burial fluxes, achieving a steady-state typically takes much longer (20 to 400 years) than in Fig. 3. In some cases, such as in curve 4 in Fig. 8, the rate of increase in phosphorus efflux is accelerated at some point in time, after the sediment retention capacity for phosphorus is exceeded.

An interesting phenomenon of bistability was observed (Fig. 8), whereby two steady-states coexisted for the same parameter set. For example, after the phosphorus efflux increased following the decrease in the interface oxygen concentration from 0.1 mM to 0.005 mM (curve 1 in Fig. 8), restoring the oxygen concentration to its original value 0.1 mM did not result in the original low value of the phosphorus flux (curve 2). Because the phosphorus efflux (Φ_{out}) is not directly constrained by the phosphorus input (Φ_{ext}), two different diagenesis regimes (one with low phosphorus efflux and one with high phosphorus efflux) could coexist for the same set of external conditions (i.e. for the same net substance inputs and interface aqueous concentrations). Incidentally, the conceptual possibility of bistability in the context of phosphorus cycling was presented by Gächter and Imboden (1985). After a prolonged anoxia (curve 1), the large amount of phosphorus cycling across the sediment–water interface generated such high sedimentation flux F_{OM} of reactive organic carbon that, even when the concentration of oxygen was restored in the bottom water, the oxic layer was too thin to limit the dissolved phosphate gradient within the sediment. These simulations suggest, in particular, that it may not be possible to reduce P efflux from sediment after a prolonged period of eutrophication only by curtailing external phosphorus inputs into the lake or by oxygenating the lake hypolimneon, and that additional measures may need to be taken to achieve the desired diagenetic regime.

Because of numerical difficulties and complications arising from bistability, we were unable to complete a full 2^k analysis for this type of boundary condition. The obtained partial results of the factorial analysis (not shown) are generally similar to those presented above for the case without the water-column phosphorus recycling: The effects of the adsorption factors are
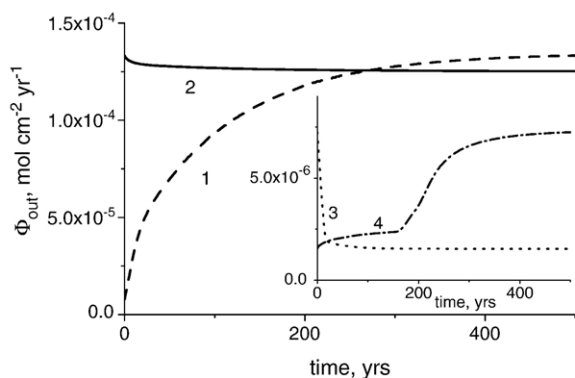
Fig. 8. Approach to a steady-state when phosphorus and iron are recycled in the water column and re-deposited to the sediment (Fig. 1b). Time evolution of the phosphorus efflux from sediment Φ_{out} is plotted after the system is perturbed from a steady-state. The perturbations are the same as in Fig. 3.

negligible, whereas the effects of phosphorus burial are crucial. The most significant factors are again F_{OM}, $[O_2]^0$, $[SO_4]^0$, and $F_{Fe(OH)3}$, and also kinetic constants k_{SFe3}, k_{FeSOx}, and k_{FeSHS}. The residuals, however, were not normally distributed, which indicates that the model response is strongly nonlinear (bistability) in the considered parameter range and therefore the factor analysis results are less reliable than for fixed Φ_{sed}.

The recycling of sediment substances in the water column makes phosphorus release flux Φ_{out} more sensitive to the variations in sediment characteristics by introducing feedbacks into the system: An increase in Φ_{out} leads to an increase in OM sedimentation flux, which increases the amount of organic phosphorus and the rates of oxygen and ferric oxyhydroxide consumption in the sediment, which, in turn, further increases Φ_{out}. Fig. 9 plots steady-state Φ_{out} against the sediment–water interface oxygen and sulfate concentrations for the two types of boundary conditions. Because the steady-state Φ_{out} is not constrained by the phosphorus input flux when the released phosphorus can be recycled, Φ_{out} reaches extremely high values for small $[O_2]^0$ and large $[SO_4^{2-}]^0$. The critical oxygen (sulfate) concentration at which the sediment is no longer able to retain phosphorus varies with the concentration of sulfate (oxygen) and the sedimentation flux of organic matter. The very high Φ_{out} values (up to 10^{-4} mol cm^{-2} yr^{-1}) obtained in our simulations, in practice, mean that the biological production in the water column switches from being phosphorus-limited to being limited by other substances, such as nitrogen. When phosphorus recycling in the water column is negligible, the efflux Φ_{out} from sediment is limited by Φ_{sed} (Fig. 9).

5.5. The role of sulfur

Our simulations confirm previous hypotheses (Caraco et al., 1993; Roden and Edmonds, 1997) that the presence of sulfate enhances long-term phosphorus effluxes (Figs. 7 and 8). For fixed phosphorus input flux Φ_{sed}, the steady-state phosphorus efflux Φ_{out} for $[SO_4]^0 = 0.2$ mM is about twice its value in an otherwise identical non-sulfidic system (curve 1 of Fig. 9b). When phosphorus recycling in the water column is substantial, increasing sulfate concentration in the bottom water can cause dramatic increase in the long-term phosphorus efflux. The fact that the magnitude of the sulfate effect on phosphorus efflux depends on the combination of several other factors, such as oxygen concentration and the organic carbon sedimentation rate (Fig. 5), explains the lack of clear cross-system correlations (Caraco et al., 1993) between the rate of sediment sulfate reduction and water-column phosphate accumulation.
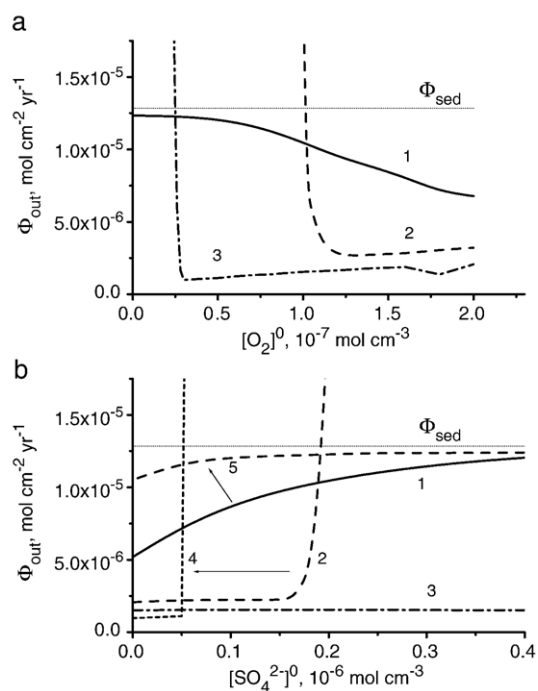

Fig. 9. The effects of interface oxygen and sulfate concentrations on phosphorus efflux from sediment. Steady-state values of phosphorus efflux from sediment are plotted against oxygen (a) and sulfate (b) concentrations at the sediment–water interface. 1,5) the total sedimentation flux of phosphorus Φ_{sed} was specified at the model's boundary (Fig. 1a). 2–4) the net external flux Φ_{ext} was specified (Fig. 1b). 1,2,4,5) The parameters (except the varied $[O_2]^0$, or $[SO_4]^0$ or F_{OM}) are as in Table 3. 3) F_{OM} is halved from its value in Table 3. 4,5) Oxygen concentration at the interface $[O_2]^0$ was set to 0 (anoxia). The arrows indicate the direction of change from oxic to anoxic conditions.

Our simulations suggest that dissolved sulfate affects the steady-state phosphorus efflux Φ_{out} by regulating the phosphorus immobilization with ferrous iron (e.g., by iron-phosphate precipitation). The primary mechanism for the sulfate–iron–phosphorus interaction is a direct dissolution of vivianite (or equivalent iron-phosphate phase) by hydrogen sulfide (reaction 10 in Table 1). This is evidenced, for example, by the large effect of the corresponding rate constant k_{Sviv} (Fig. 5). For $k_{Sviv} > 10^8$ cm^3/mol/yr, the rate of the sulfide-induced dissolution of vivianite was limited in our simulations by the amount of available sulfide. We are unaware of any independent estimates of the k_{Sviv} value. In all our simulations, the rate of vivianite precipitation exceeded the rate of its H$_2$S-induced dissolution because of sufficiently high porewater concentrations [Fe^{2+}] and [H$_3$PO$_4$].

The other two mechanisms discussed above (dissolution of Fe(III) solids by hydrogen sulfide and prevention of ferrous phosphates formation by FeS precipitation) for the sulfate-assisted phosphorus release were insignificant in our simulations. Vivianite precipitation was only slightly affected by the Fe^{2+} binding in FeS; setting $k_{FeS} = 0$ (reaction 12) affected Φ_{out} by less than 0.01%. The direct dissolution of Fe (III) oxyhydroxides by H$_2$S was also unimportant: The curves in Fig. 8b were unaffected by setting $k_{Fe3HS} = 0$. We could not verify the importance of preferential dissolution of siderite (over vivianite) by H$_2$S (as suggested in (Gächter and Müller, 2003)) because of a too small amount of FeCO$_3$ (siderite) generated in most simulations.

A counter-intuitive result was obtained for a case where a substantial amount of solid Fe(III) survived reduction in the sediment column and was buried permanently into the deep sediment (this was achieved by increasing $C_{Fe(OH)3}^{lim}$ to effectively inhibit bacterial iron reduction). Whereas one could expect that enhancing sulfide-induced dissolution of Fe(OH)$_3$ (reaction 9) would increase phosphorus efflux by releasing sorbed P into the porewater, the Φ_{out} efflux, in fact, decreased with increasing k_{SFe3}. Similarly to the small role of phosphorus sorption parameters discussed above, this contradiction is explained by the dominant role of phosphorus burial in the steady-state: The Fe^{2+} and phosphate ions released into the porewater increase the rate of vivianite precipitation, which overcompensates for the loss in sediment sorption capacity.

The enhancement of phosphorus mobilization in the presence of dissolved sulfate in our simulations suggests that the loading of sulfur into lakes (e.g., as acid rain) may, under many conditions (e.g., in hypoxic iron-rich lakes), exacerbate phosphorus releases from sediments and lead to eutrophication (Caraco et al., 1989). A more careful analysis is needed to take into account the effect of sulfate on other ecosystem parameters, since the associated changes in the pH or the biological productivity of the water column may have an opposite effect on the phosphorus release rates (Curtis, 1989).

6. Summary

Using a reactive-transport model, we have investigated a lake sediment system for characteristics that control long-term (steady-state) phosphorus effluxes from sediment into the water column. Our modeling exploration included the reactions and processes of the classical model of Einsele (1936) and Mortimer (1941) and the recently suggested (Caraco et al., 1993; Roden and Edmonds, 1997) reactions by which phosphorus effluxes can be affected by the dissolved sulfate concentration in the overlying water. Our main conclusions are:

1) Long-term phosphorus efflux from sediments is predominantly controlled by *combinations* of the following factors: the concentrations of dissolved oxygen and sulfate at the sediment–water interface, the rate of phosphorus immobilization in reduced sediment, the sedimentation flux of reactive ferric iron, and the sedimentation flux of organic matter, the latter being most important of all.
2) Which phosphorus release mechanisms are relevant depends on the time scale of interest. The mechanisms implicated in short-term laboratory or in-situ studies cannot in general be extrapolated to long-term phosphorus retention in natural sediments. Since the classical model was originally formulated for phosphorus releases during seasonal anoxia, remediation measures based on the classical model, such as artificial hypolimneon oxygenation, can have only short-lasting effect. Precipitation and permanent burial of phosphorus-bearing solid phases (rather than phosphorus sorption near the sediment–water interface) are key to phosphorus retention in the long-term. Further research is needed to experimentally quantify the mineralogy and the rate of formation and dissolution of the relevant phases occurring below the oxygen penetration depth.
3) Dissolved sulfate increases phosphorus effluxes from sediments, primarily by the dissolution of phosporus-bearing phases by hydrogen sulfide generated in the process of microbial sulfate reduction.

4) Higher oxygen concentrations in the overlying waters generally decrease phosphorus effluxes from sediments. This effect of oxygen concentration on sediment phosphorus retention is diminished, however, in the presence of sulfate.

5) Recycling of released phosphorus back to the sediment (via water-column productivity and organic carbon sedimentation) introduces positive feedbacks that strongly affect the sediment system response to changing external conditions. Model calculations demonstrate the possibility of bistability, whereby two steady-states are possible and the trophic state of the sediment–water-column system depends not only on the system's characteristics but also on its history. This suggests that the task of decreasing sediment phosphorus effluxes after a prolonged period of eutrophication can require more than the restoration of pre-eutrophic phosphorus inputs and hypolimnetic O_2 concentrations.

Acknowledgements

References

Alfaro-De la Torre, Ma.C., Tessier, A., 2002. Cadmium deposition and mobility in the sediments of an acidic oligotrophic lake. Geochim. Cosmochim. Acta 66, 3549–3562.

Balistrieri, L.S., Murray, J.W., 1981. The surface chemistry of δ-MnO_2 in major ion seawater. Geochim. Cosmochim. Acta 46, 1041–1052.

Berner, R.A., 1980. Early Diagenesis: A Theoretical Approach. Princeton Series in Geochemistry. Princeton Univ. Press.

Boers, P.C.M., Van Raaphorst, W., Van der Molen, D.T., 1998. Phosphorus retention in sediments. Water Sci. Technol. 37 (3), 31–39.

Boström, B., Jansson, M., Forsberg, C., 1982. Phosphorus release from lake sediments. Arch. Hydrobiol., Beih. Ergebn. Limnol. 18, 5–59.

Boström, B., Andersen, J.M., Fleischer, S., Jansson, M., 1988. Exchange of phosphorus across the sediment–water interface. Hydrobiologia 170, 229–244.

Boudreau, B.P., 1996. A method-of-lines code for carbon and nutrient diagenesis in aquatic sediments. Comput. Geosci. 22, 479–496.

Boudreau, B.P., 1997. Diagenetic Models and Their Implementation. Springer.

Brown, P.N., Byrne, G.D., Hindmarsh, A.C., 1989. VODE, a variable-coefficient ODE solver. SIAM J. Sci. Statist. Comput. 10, 1038–1051.

Brun, R., Reichert, P., Künsch, H.R., 2001. Practical identifiability analysis of large environmental simulation models. Water Resour. Res. 37, 1015–1030.

Caraco, N.F., Cole, J.J., Likens, G.E., 1989. Evidence for sulphate-controlled phosphorus release from sediments of aquatic systems. Nature 341, 316–318.

Caraco, N.F., Cole, J.J., Likens, G.E., 1991. Phosphorus release from anoxic sediments: lakes that break the rules. Verh. Int. Ver. Limnol. 24, 2985–2988.

Caraco, N.F., Cole, J.J., Likens, G.E., 1993. Sulfate control of phosphorus availability in lakes. Hydrobiologia 253, 275–280.

Carignan, R., Lean, D.R.S., 1991. Regeneration of dissolved substances in a seasonally Anoxic Lake: the relative importance of processes occurring in the water column in the sediments. Limnol. Oceanogr. 36, 683–707.

Carignan, R., Tessier, A., 1988. The co-diagenesis of sulfur and iron in acid lake sediments of southwestern Quebec. Geochim. Cosmochim. Acta 52, 1179–1188.

Carlton, R.G., Wetzel, R.G., 1988. Phosphorus flux from lake sediments: effect of epipelic algal oxygen production. Limnol. Oceanogr. 33, 562–570.

Curtis, P.J., 1989. Effects of hydrogen ion and sulphate on the phosphorus cycle of a Precambrian Shield lake. Nature 337, 156–158.

Davison, W., 1993. Iron and manganese in lakes. Earth-Sci. Rev. 34, 119–163.

Einsele, W., 1936. Ueber die Beziehungen des Eisenkreislaufs zum Phosphatekreislauf um eutrophen See. Arch. Hydrobiol. 29, 664–686.

Elliott, M., Zheng, Y., Bagley, D.M., 2000. Determining significant anaerobic kinetic parameters using simulation. Environ. Technol. 21, 1181–1191.

Emerson, S., Widmer, G., 1978. Early diagenesis in anaerobic lake sediments: II. Thermodynamic and kinetic factors controlling the formation of iron phosphate. Geochim. Cosmochim. Acta 42, 1307–1316.

Fossing, H., Berg, P., Thamdrup, B., Rysgaard, S., Sorensen, H.M., Nielsen, K., 2004. A model set-up for an oxygen and nutrient flux model for Aarhus Bay (Denmark). NERI Technical Report, vol. 483.

Friedl, G., Wehrli, B., Manceau, A., 1997. Solid phases in the cycling of manganese in eutropic lakes: new insights from EXAFS spectroscopy. Geochim. Cosmochim. Acta 61, 275–290.

Froelich, P.N., Klinkhammer, G.P., Bender, M.L., Luedtke, G.R., Heath, G.R., Cullen, D., Dauphin, P., 1979. Early oxidation of organic matter in pelagic sediments of the eastern equatorial Atlantic: suboxic diagenesis. Geochim. Cosmochim. Acta 43, 1075–1090.

Fürrer, Wehrli, 1996. Microbial reactions, chemical speciation, and multicomponent diffusion in porewaters of a eutropic lake. Geochim. Cosmochim. Acta 60, 2333–2346.

Gächter, R., Imboden, D., 1985. Lake restauration. In: Stumm, W. (Ed.), Chemical Processes in Lakes. InJohn Wiley and Sons, pp. 365–388.

Gächter, R., Müller, B., 2003. Why the phosphorus retention of lakes does not necessarily depend on the oxygen supply to their sediment surface. Limnol. Oceanogr. 48, 929–933.

Gächter, R., Wehrli, B., 1998. Ten years of artificial mixing and oxygenation: no effect on the internal phosphorus loading in two eutrophic lakes. Environ. Sci. Technol. 32, 3659–3665.

Gächter, R., Meyer, J.S., Mares, A., 1988. Contribution of bacteria to release and fixation of phosphorus in lake sediments. Limnol. Oceanogr. 33, 1542–1558.

Golterman, H.L., 1995. The role of the ironhydroxide–phosphate–sulphide system in the phosphate exchange between sediments and overlying water. Hydrobiologia 297, 43–54.

Golterman, H.L., 2001. Phosphate release from anoxic sediments or "What did Mortimer really write?". Hydrobiologia 450, 99–106.

Hecky, R.E., Campbell, P., Hendzel, L.L., 1993. The stoichiometry of carbon, nitrogen, and phosphorus in particulate matter of lakes and oceans. Limnol. Oceanogr. 38, 709–724.

Holdren Jr., G.C., Armstrong, D.E., 1980. Factors affecting phosphorus release from intact lake sediment cores. Environ. Sci. Technol. 14, 79–87.

Holmer, M., Storkholm, P., 2001. Sulphate reduction and sulphur cycling in lake sediments: a review. Freshw. Biol. 46, 431–451.

Hornberger, G., Spear, R., 1981. An approach to the preliminary analysis of environmental systems. J. Environ. Manag. 12, 7–18.

House, W.A., Casey, H., Donaldson, L., Smith, S., 1986. Factors affecting the coprecipitation of inorganic phosphate with calcite in hardwaters: I. Laboratory studies. Water Res. 20, 917–922.

Hunter, K.S., Wang, Y., Van Cappellen, P., 1998. Kinetic modeling of microbially-driven redox chemistry of subsurface environments: coupling transport, microbial metabolism and geochemistry. J. Hydrol. 209, 53–80.

Hupfer, M.R., Gächter, R., Giovanoli, R., 1995. Transformation of phosphorus species in settling seston and during early sediment diagenesis. Aquat. Sci. 57, 305–324.

Jackson, T.A., Schindler, D.W., 1975. The biogeochemistry of phosphorus in an experimental lake environment: evidence for the formation of humic–metal–phosphate complexes. Verh. Int. Ver. Limnol. 19, 211–221.

Jensen, H.S., Kristensen, P., Jeppesen, E., Skytthe, A., 1992. Iron: phosphorus ratio in surface sediment as an indicator of phosphate release from aerobic sediments in shallow lakes. Hydrobiologia 235–236, 731–743.

Jourabchi, P., Van Cappellen, P., Regnier, P., 2005. Quantitative interpretation of pH distributions in aquatic sediments: a reaction-transport modeling approach. Am. J. Sci. 305, 919–956.

Kalff, J., 2002. Limnology: Inland Water Ecosystems. Prentice Hall.

Katsev, S., Rancourt, D.G., L'Heureux, I., 2004. dSED: a database tool for modeling sediment early diagenesis. Comput. Geosci. 30, 959–967.

Katsev, S., Sundby, B., Mucci, A., 2006. Modeling vertical migrations of the redox boundary in sediments: application to deep basins of the Arctic Ocean. Limnol. Oceanogr. 51, 1581–1593.

Kliza, D., Telmer, K., 2001. Phase I: lake sediment studies in the vicinity of the Horne smelter in Rouyn-Noranda, Quebec, GSC-Openfile 2952, July 2001.

Lasaga, A.C., 1998. Kinetic Theory in the Earth Science. Princeton University Press, Princeton.

Lewandowski, J., Rüter, K., Hupfer, M., 2002. Two-dimensional small-scale variability of pore water phosphate in freshwater lakes: results from a novel dialysis sampler. Environ. Sci. Technol. 36, 2039–2047.

Manning, P.G., Murphy, T.P., Prepas, E.E., 1991. Intensive formation of vivianite in the bottom sediments of mesotrophic Narrow Lake, Alberta. Can. Mineral. 29, 77–85.

Manning, P.G., Prepas, E.E., Serediak, M.S., 1999. Pyrite and vivianite intervals in the bottom sediments of eutrophic Baptiste Lake, Alberta, Canada. Can. Mineral. 37, 593–601.

Meysman, F.J.R., Middelburg, J.J., Herman, P.M.J., Heip, C.H.R., 2003. Reactive transport in surface sediments. II. Media: an object-oriented problem-solving environment for early diagenesis. Comput. Geosci. 29, 301–318.

Montgomery, D.C., 1997. Design and Analysis of Experiments. John Wiley and Sons, New York.

Morris, M.D., 1991. Factorial sampling plans for preliminary computational experiments. Technometrics 33, 161–174.

Morse, J.W., Millero, F.J., Cornwell, J.C., Rickard, D., 1987. The chemistry of the hydrogen sulfide and iron sulfide systems in natural waters. Earth-Sci. Rev. 24, 1–42.

Mortimer, C.H., 1941. The exchange of dissolved substances between mud and water in lakes. J. Ecol. 29, 280–329.

Nriagu, J.O., Dell, C.I., 1974. Diagenetic formation of iron phosphates in recent lake sediments. Am. Mineral. 59, 934–946.

Omlin, M., Brun, R., Reichert, P., 2001. Biogeochemical model of lake Zurich: sensitivity, identifiability and uncertainty analysis. Ecol. Model. 141, 105–123.

Parfitt, R.L., 1989. Phosphate reactions with natural allophane, ferrihydrite, and goethite. J. Soil Sci. 40, 359–369.

Postma, D., Jakobsen, R., 1996. Redox zonation: equilibrium constraints on the $Fe(III)/SO_4$ — reduction interface. Geochim. Cosmochim. Acta 17, 3169–3175.

Prairie, Y.T., de Montigny, C., Del Giorgio, P.A., 2001. Anaerobic phosphorus release from sediments: a paradigm revisited. Verh. Int. Ver. Limnol. 27, 4013–4020.

Reichert, P., Schervish, M., Small, M.J., 2002. An efficient sampling technique for Bayesian inference with computationally demanding models. Technometrics 44, 318–427.

Rickard, D., 1997. Kinetics of pyrite formation by the H_2S oxidation of iron (II) monosulfide in aqueous solutions between 25 and 125 C: the rate equation. Geochim. Cosmochim. Acta 61, 115–134.

Roden, E.E., Edmonds, J.W., 1997. Phosphate mobilization in iron-rich anaerobic sediments: microbial Fe(III) oxide reduction versus iron-sulfide formation. Arch. Hydrobiol. 139, 347–378.

Rudd, J.W.M., Kelly, C.A., Furutani, A., 1986. The role of sulfate reduction in long term accumulation of organic and inorganic sulfur in lake sediments. Limnol. Oceanogr. 31, 1281–1291.

Saltelli, A., Chan, K., Scott, E.M. (Eds.), 2000. Sensitivity Analysis. InJohn Wiley and Sons, Chichester.

Schauser, I., Lewandowski, J., Hupfer, M., 2003. Decision support for the selection of an appropriate in-lake measure to influence the phosphorus retention in sediments. Water Res. 37, 801–812.

Schauser, I., Hupfer, M., Brüggemann, R., 2006. Sensitivity analysis with a phosphorus diagenesis model (SPIEL). Ecol. Model. 190, 87–98.

Soetaert, K., Herman, P.M.J., Middelburg, J.J., 1996. Dynamic response of deap-sea sediments to seasonal variations: a model. Limnol. Oceanogr. 41, 1651–1668.

Soetaert, K., Middelburg, J.J., Herman, P.M.J., Buis, K., 2000. On the coupling of benthic and pelagic biogeochemical models. Earth-Sci. Rev. 51, 173–201.

Søndergaard, M., Jensen, J.P., Jeppesen, E., 2001. Retention and internal loading of phosphorus in shallow, eutrophic lakes. Sci. World 1, 427–442.

Tromp, T.K., Van Cappellen, P., Key, R.M., 1995. A global model for the early diagenesis of organic carbon and organic phosphorus in marine sediments. Geochim. Cosmochim. Acta 59, 1259–1284.

Urban, N.R., 1994. Environmental Chemistry of Lakes and Reservoirs. American Chemical Society, pp. 323–369.

Van Cappellen, P., Wang, Y., 1995. Metal cycling in surface sediments: modeling the interplay between transport and reaction. In: Allen, H.E. (Ed.), Metal Speciation and Contamination of Aquatic Sediments. InAnn Arbor Press, pp. 21–64.

Van Cappellen, P., Wang, Y., 1996a. Cycling of iron and manganese in surface sediments: a general theory for the coupled transport and

reaction of carbon, oxygen, nitrogen, sulfur, iron, and manganese. Am. J. Sci. 296, 197–243.

Van Cappellen, P., Wang, Y., 1996b. A multicomponent reactive transport model of early diagenesis: application to redox cycling in coastal marine sediments. Geochim. Cosmochim. Acta 60, 2993–3014.

Wang, H., Appan, A., Gulliver, J.S., 2003. Modeling of phosphorus dynamics in aquatic sediments: II. Examination of model performance. Water Res. 37, 3939–3953.

Wersin, P., Hohener, P., Giovanoli, R., Stumm, W., 1991. Early diagenetic influences on iron transformations in a freshwater lake sediment. Chem. Geol. 90, 233–252.

Wetzel, R.G., 2001. Limnology. Academic Press.

Wieringa, E.B.A., Overmann, J., Cypionka, H., 2000. Detection of abundant sulphate-reducing bacteria in marine oxic sediment layers by a combined cultivation and molecular approach. Environ. Microbiol. 2, 417–427.

Wijsman, J.W.M., Herman, P.M.J., Middelburg, J.J., Soetaert, K., 2002. A model for early diagenesis processes in sediments of the continental shelf of the Black Sea. Estuar. Coast. Shelf Sci. 54, 403–421.

Williams, J.D.H., Syers, J.K., Shukla, S.S., Harris, R.F., Armstrong, D.E., 1971. Levels of inorganic and total phosphorus in lake sediments as related to other sediment parameters. Environ. Sci. Technol. 5, 1113–1120.